Tetrameric UvrD helicase is located at the *E. coli* replisome due to frequent replication blocks

Adam J. M Wollman[1,2,3,], Aisha H. Syeda[1,2], Jamieson A. L. Howard[1,2], Alex Payne-Dwyer[1,2], Andrew Leech[4] , Colin Guy[5, 6], Peter McGlynn[2,6], Michelle Hawkins[2] and Mark C. Leake[1,2]

The authors wish it to be known that, in their opinion, the first two authors should be regarded as joint First Authors

[1] School of Physics, Engineering and Technology, University of York, York YO10 5DD, United Kingdom.

[2] Department of Biology, University of York, York YO10 5DD, United Kingdom.

[3] Current address: Biosciences Institute, Newcastle University, NE1 7RU, United Kingdom.

[4] Bioscience Technology Facility, Department of Biology, University of York, York YO10 5DD, United Kingdom

[5] Current address: Covance Laboratories Ltd., Otley Road, Harrogate, HG3 1PY, United Kingdom

[6] Previous address: School of Medical Sciences, Institute of Medical Sciences, University of Aberdeen, Foresterhill, Aberdeen AB25 2ZD, United Kingdom

* To whom correspondence should be addressed. To whom correspondence should be addressed. Tel: +44 (0)1904322697. Email: mark.leake@york.ac.uk

Present Address: School of Physics, Engineering and Technology, and Department of Biology, University of York, York YO10 5DD, United Kingdom

SUMMARY

DNA replication in all organisms must overcome nucleoprotein blocks to complete genome duplication. Accessory replicative helicases in *Escherichia coli*, Rep and UvrD, help replication machinery overcome blocks by removing incoming nucleoprotein complexes or aiding the re-initiation of replication. Mechanistic details of Rep function have emerged from recent live cell studies; however, the division of UvrD between its multiple activities in DNA repair and its role as an accessory helicase remains unclear in live cells. Here, by integrating super-resolved single-molecule fluorescence microscopy with biochemical analysis, we find that UvrD self-associates into tetrameric assemblies and, unlike Rep, is not recruited to a specific replisome protein despite being found at approximately 80% of replication forks. Instead, its recruitment to forks is likely mediated by the very high frequency of replication blocks due to DNA bound proteins, including RNA polymerase and DNA damage. Deleting *rep* and DNA repair factor genes *mutS* and *uvrA*, and inhibiting transcription through

RNA polymerase mutation and antibiotic inhibition, indicates that the level of UvrD at the fork is dependent on its function. Our findings show that UvrD is recruited to sites of nucleoprotein blocks via distinctly different mechanisms to Rep and plays a multi-faceted role in ensuring successful DNA replication.

INTRODUCTION

Replication and transcription of DNA occur simultaneously in *Escherichia coli,* making conflicts between the bacterial replisome, the molecular replication machine comprising in excess of 10 different proteins, and RNA polymerase (RNAP) inevitable (1–4). Collisions between the replication and transcription machineries hinder replication fork progression and cause genome instability (5–14). RNAP can pause, stall and backtrack while actively transcribing, and any immobile RNAP molecules present long-lived barriers to replisomes (15, 16). These factors make RNAP the most common nucleoprotein obstacle for translocating replisomes. DNA is also frequently damaged in normal growth conditions due to exposure to endogenous and exogenous DNA damaging agents. The resulting DNA damage also presents significant obstacles for normal replication (17–19).

Several mechanisms exist to reduce conflict between the replisome and obstacles such as transcribing RNAPs. For example, transcription elongation and termination factors reduce the number of immobile RNA polymerases on DNA (1, 18, 20–24). Head-on collisions were originally thought to be more harmful (25–27) and therefore more important to resolve; a view supported by the occurrence of highly transcribed genes encoded on the leading strand, presumably to ensure co-directional transcription and replication (26, 28, 29). However, co-directional collisions of the replisome and transcription machinery also impact replication fork progression (3, 18, 30).

Accessory replicative helicases promote fork movement through nucleoprotein barriers and have been identified in prokaryotes and eukaryotes (1, 12, 13, 31, 32). The Rep and UvrD accessory helicases in *E. coli*, as well as the Pif1 helicase in *Saccharomyces cerevisiae*, perform important roles in helping to clear nucleoprotein complexes (33). More recently, Pif1 has been proposed to be a general displacement helicase for replication bypass of protein blocks, a function similar to the Rep and UvrD helicases (34). These helicases can reduce replisome pausing at several types of

70 native transcription complexes observed in living cells (13, 22, 35), and several types
71 of engineered nucleoprotein blocks in biochemical experiments *in vitro* (1, 31).
72 Rep is the primary accessory helicase in *E. coli*, however, UvrD can partially
73 compensate for the absence of Rep *in vivo* and has been shown to promote replication
74 through stalled transcription elongation complexes (1, 12, 13, 36, 37). UvrD is a
75 superfamily 1 helicase that translocates 3'-5' along ssDNA. The ability of UvrD to
76 compensate partially for the absence of Rep has been attributed to the high degree of
77 homology between these two helicases and the abundance of UvrD inside cells (12,
78 21, 38–40). The role of UvrD in nucleotide excision repair along with UvrABC proteins
79 as well as in methyl-directed mismatch repair along with the MutHLS proteins is well
80 characterised (41–46). UvrD interacts directly with RNAP but the functional
81 importance of this interaction has been unclear until recently (47–50). UvrD has been
82 suggested to promote backtracking of stalled RNAP as a first step in transcription-
83 coupled repair (50, 51); however, other studies argue against UvrD playing any role in
84 coupling nucleotide excision repair to stalled transcription complexes (48, 49, 52–56).
85 Here, we combined state-of-the-art live cell imaging using single-molecule
86 microscopy with advanced biochemical activity experiments *in vitro* to elucidate how
87 UvrD resolves replicative blocks. We used super-resolved high-speed single-molecule
88 fluorescence microscopy of mGFP-UvrD in live cells co-expressing a fork marker,
89 DnaQ-mCherry, to reveal that 80% of DnaQ foci colocalise with UvrD. Stepwise
90 photobleaching intensity analysis revealed tetrameric UvrD foci *in vivo*, to be
91 compared with earlier observations performed *in vitro* using analytical
92 ultracentrifugation that found a mixture of UvrD dimers and tetramers (57). Surface
93 plasmon resonance (SPR) measurements of UvrD in combination with each replisome
94 component identified no specific replisome protein interaction partner that would
95 explain replisome-UvrD colocalisation. Deletion of Rep, mismatch repair protein MutS
96 and nucleotide excision repair protein UvrA, and disruption of transcription using either
97 mutation of RNAP or antibiotic inhibition, significantly reduces the number of UvrD or
98 level of observed colocalisation of UvrD with the fork. Coupled with *in vitro* block-
99 dependent differences in UvrD replication promotion efficiency, we conclude that UvrD
100 is located at the *E. coli* replisome due to its role in resolving frequent blocks to
101 replication.
102
103

RESULTS

UvrD is present at the majority of replication forks

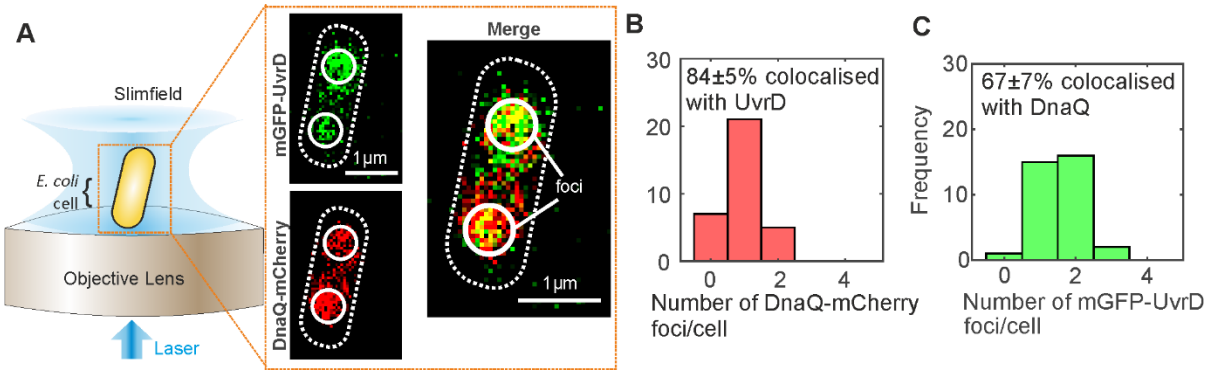

Figure 1: Super-resolved single-molecule light microscopy. (A). Slimfield microscope schematic and Slimfield micrographs of mGFP-UvrD, DnaQ-mCherry. Cell membrane and DnaQ/UvrD foci indicated as white dashed and non-dashed lines respectively. (B) and (C) Histogram showing the number of DnaQ and UvrD foci detected per cell respectively, SD errors. N=45 cells.

We investigated the role of UvrD in DNA replication using super-resolved single-molecule fluorescence microscopy to track dynamic patterns of fluorescently labelled UvrD localization relative to the replication fork in live cells (Figure 1A). We performed dual-colour Slimfield (63, 78) to assess the degree of colocalisation between UvrD and the replisome, using the same imaging protocol we used previously to confirm Rep colocalisation with the replisome(13). We employed DnaQ-mCherry as a fork marker (13) along with a genomically integrated mGFP-UvrD fluorescent protein fusion construct to report on the localization of UvrD. DnaQ encodes the epsilon subunit, a core component of the DNA polymerase and is well established as a marker for the replication fork (13, 69, 79–81). These strains phenocopied the wild type strain for growth and in plasmid loss assays testing for mGFP-UvrD function retention (Supplementary Figures S1, S2, Tables S1-4). The helicase activity of mGFP-UvrD was comparable to the wild type enzyme in an *in vitro* unwinding assay (Supplementary Figure S3). Under Slimfield, we observed 1-2 DnaQ foci as in the previous study for Rep, corresponding to the two moving replication forks which appear as single foci near the start of replication when they are separated by less than the 200-300 nm diffraction limit of our microscope (Figure 1A,B Supplementary Figure S4). We also observed 1-2 UvrD foci per cell, of which 67 ± 7% (±SEM) were colocalised with DnaQ foci and 84 ± 5% of DnaQ foci were colocalised with UvrD (Figure 1B and C). We calculated the probability of random overlap between these

133 foci, by modelling the nearest-neighbour foci separation as a Poisson distribution (70),
134 to be 20%. To confirm that colocalisation between DnaQ and UvrD was not just a
135 function of the nucleoid association of UvrD, we performed Slimfield imaging of Heat-
136 stable nucleoid-structuring protein (H-NS) tagged with GFP dual labelled with DnaQ-
137 mCherry. H-NS associates with the nucleoid but not specifically with the fork. We
138 found similar numbers of H-NS foci to UvrD foci (Supplementary Figure S5) but only
139 38±4% DnaQ foci were colocalised with H-NS implying that, similarly to the Rep
140 helicase (13), UvrD is present at the majority of replication forks.
141
142 **UvrD foci are tetrameric assemblies in live bacterial cells**
143

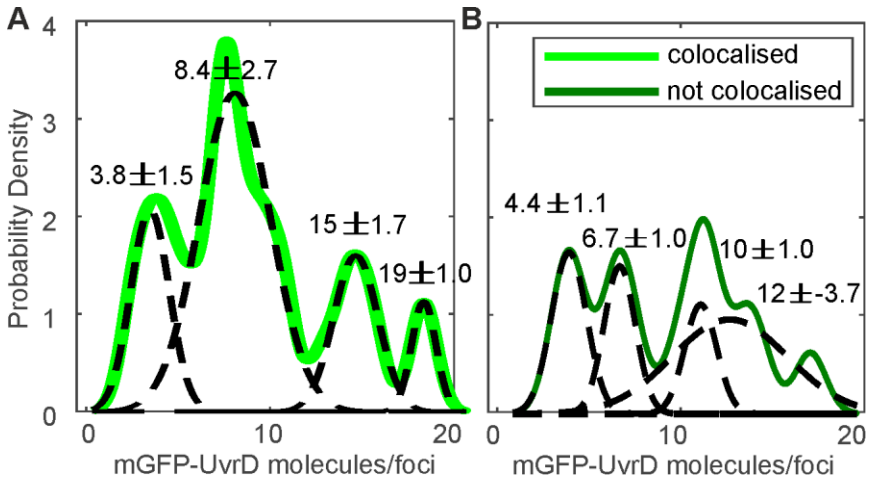

144
145 **Figure 2 UvrD stoichiometry.** The distribution of UvrD foci stoichiometry rendered as a
146 kernel density estimate for foci colocalised (A) and not colocalised (B) with DnaQ foci.
147 Distributions were fitted with multiple Gaussian peaks (black dotted lines) with the peak value
148 ± error determined by the half width at half maximum indicated above each peak
149
150 Slimfield also enabled the stoichiometry of these foci to be determined by utilizing a
151 method involving step-wise photobleaching analysis (69). Here, we determined the
152 brightness of a single-molecule of mGFP or mCherry fluorescent protein under our
153 Slimfield imaging conditions (Supplementary Figure S7), and used these values to
154 normalize the initial brightness of all tracked foci as an estimate for the apparent
155 stoichiometry in terms of number of fluorescently labelled molecules present. We
156 found that DnaQ had the same range of 2-6 molecules per focus (Supplementary
157 Figure S8) as we have found previously, corresponding to 2-3 polymerases per fork
158 (13, 69). The distribution of the apparent stoichiometry of UvrD foci which are
159 colocalised with DnaQ had a distinct lowest-order peak corresponding to

160 approximately four molecules, with subsequent peaks at clear multiples of four (Figure
161 2A). UvrD foci that are not colocalised with DnaQ also contained a distinct lowest-
162 order peak at four, but subsequent peaks were less clearly tetrameric. We performed
163 Size Exclusion Chromatography - Multi-Angle Laser Light Scattering (SEC-MALLS) to
164 test whether the fluorescent protein labelling UvrD might be inducing multimers but
165 found limited effects on UvrD assembly state, as expected from the K_D dissociation
166 constant of fluorescent proteins containing the A206K mutation (82) (Supplementary
167 Figure S9). UvrD has been shown to exist in a monomer-dimer-tetramer equilibrium
168 *in vitro* (57). DNA unwinding experiments *in vitro* suggest UvrD must function as at
169 least a dimer (83) or a trimer (84), however the oligomeric state of functional UvrD is
170 disputed (reviewed in (85)). Our results are consistent with UvrD existing
171 predominantly as a tetramer or a dimer of dimers, with multiple tetramers or dimer-
172 dimers sometimes present at forks. It should be noted that we often observe only a
173 single DnaQ focus corresponding to two replication forks which are separated by less
174 than the diffraction limit of our microscope (Supplementary Figure S8) such that some
175 multiple tetrameric UvrD foci correspond to two replication forks. The less distinct
176 peaks in the UvrD foci that are not colocalised with DnaQ may indicate that other UvrD
177 species (monomers, dimers or trimers) are also present.
178 We were also able to determine the total cell copy number of UvrD using a
179 method which determined the total contribution of mGFP-UvrD fluorescence to the
180 observed intensity in whole cells (72). We found approximately 800 molecules of UvrD
181 per cell (Supplementary Figure S10), similar to that which we reported previously for
182 Rep (13). This is a much lower level of UvrD than was reported using transcription rate
183 measurements (86) or high-throughput proteomics (87) but is comparable to recent
184 estimates using ribosome profiling (88).
185
186 **No interaction partner was found for UvrD at the fork with SPR**
187 Our earlier findings concerning the accessory helicase Rep indicated that
188 colocalisation with the fork and recruitment to the replisome were mediated by specific
189 interaction with the replicative helicase DnaB (89), with Rep and DnaB both exhibiting
190 hexameric stoichiometry (13, 69). We sought to determine whether UvrD is also
191 recruited by interacting with a specific replisome component using SPR on purified
192 UvrD and each replisome component (Supplementary Figure 11). UvrD (under
193 conditions consistent with predominantly monomeric UvrD as determined by SEC-

194 MALLs (Supplementary Figure S9) exhibited no direct interaction with primase, SSB,
195 β sliding clamp, the DNA polymerase III αε, χψ or γ complexes; or θ, δ, δ′, χ, and γ
196 subunits (12). We did initially identify a putative weak UvrD-Tau interaction. However,
197 as a control we also tested Rep, and found this also interacted with Tau to a similar
198 extent, and with ~100x lower affinity than UvrD with known interaction partner UvrB
199 (Supplementary Figure 8). We therefore conclude that the Tau interaction with UvrD
200 is non-specific and that, unlike Rep, UvrD likely does not have a direct interaction
201 partner at the replisome from the suite of replisome proteins tested. As UvrD is a
202 tetramer at the replisome, it is also unlikely to be recruited by Rep, which has shown
203 putative interaction (90).
204

205 **UvrD presence at the replication fork is mediated by specific blocks to**
206 **replication**

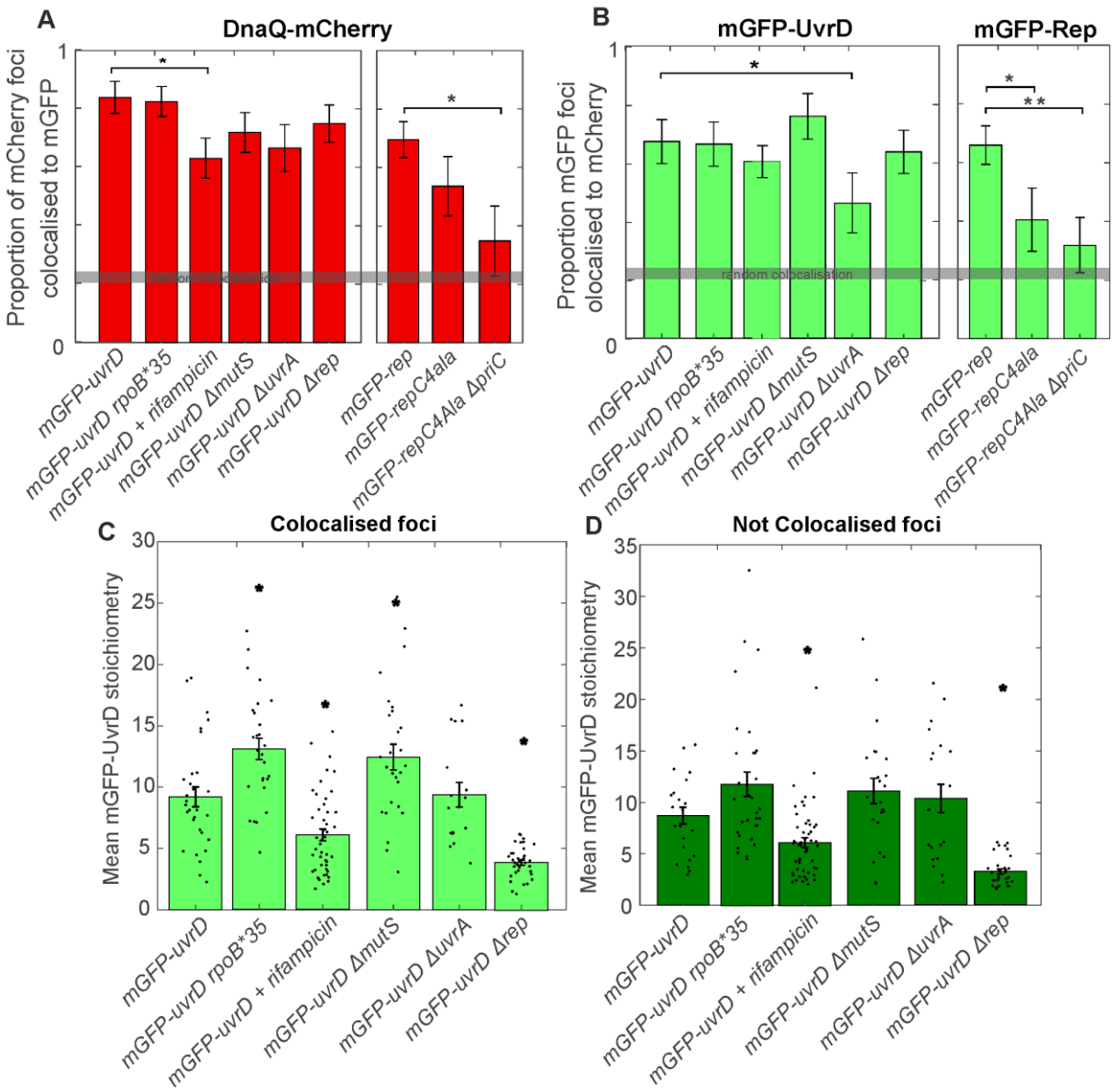

207

208 Figure 3: UvrD perturbations. A. and B. The mean proportion of colocalised DnaQ and UvrD
209 **or Rep** foci per cell respectively. Error bars represent standard error in the mean and
210 statistical significance by Brunner Munzel and Student's t-test $p<0.05$ indicated by *. Gray
211 bar indicates levels of predicted random colocalisation. C. and D. Jitter plots of colocalised
212 and not colocalised UvrD stoichiometry respectively. Bars show mean UvrD stoichiometry
213 with error bars showing the standard error in the mean and statistical significance by Brunner
214 Munzel and Student's t-tests $p<0.05$ indicated by *. N=30 cells.
215
216
217 Since our SPR observations indicated that UvrD does not interact directly and
218 specifically with any core replisome protein, we hypothesized that the association of
219 UvrD with the replication fork might be dependent on its activity in resolving

220 nucleoprotein blocks. To test this, we systematically impaired key DNA replication
221 repair processes in which UvrD is implicated, as well as perturbing RNAP replicative
222 blocks by disruption of transcription through both genetic mutation and antibiotic
223 inhibition (Figure 3). We investigated how these perturbations altered fork association
224 through levels of UvrD colocalisation with DnaQ. As a control, we compared these to
225 levels of Rep colocalisation with DnaQ which can be abrogated down to random levels
226 of colocalisation, indicating no interaction with the fork, by mutations which stop Rep
227 interacting with DnaB and PriC (Figure 3A). We perturbed UvrD's activity in resolving
228 DNA damage at replication blocks by deleting *mutS* or *uvrA*, rendering the strains
229 defective in UvrD-associated mismatch repair or nucleotide excision repair
230 respectively (43, 91). We reduced the need for UvrD to remove transcriptional blocks
231 to replication (49) by introducing the *rpoB*35* mutation, which destabilizes open
232 complexes formed during initiation of transcription (92, 93); and by using the antibiotic
233 rifampicin, which blocks elongation of RNA transcripts (94). All of these strains were
234 healthy under normal growth conditions (Supplementary Figure S1, Table S4) and
235 displayed the same phenotype for DnaQ foci number and stoichiometry within
236 measurement error (Supplementary Figure S8).
237 For the transcriptional block perturbations, the *rpoB*35* mutant dual labelled
238 strain exhibited no difference in the proportion of colocalised DnaQ or UvrD foci
239 (Figure 3A and B). This mutant and all others tested exhibited the same predominant
240 tetrameric stoichiometry trends as wild type (Supplementary Figure S12), with clear
241 peaks at tetramer intervals in the colocalised stoichiometry distribution and less clear
242 but still largely tetrameric intervals in the stoichiometry distribution for UvrD foci that
243 are not colocalised with DnaQ. This provides further evidence for tetrameric UvrD
244 assemblies *in vivo*. We compared the mean stoichiometry for each mutant to that of
245 wild type (Figure 3C and D). Unexpectedly, the *rpoB*35* mutant produced a slight but
246 statistically significant increase in mean colocalised stoichiometry, corresponding to
247 approximately one extra UvrD tetramer at the replication fork (Figure 3C). This finding
248 may indicate the level of instability conferred by this mutation has multiple downstream
249 effects that alter UvrD localisation significantly at the fork. Alternatively, it could mean
250 that *rpoB*35* does not affect the formation of the types of transcriptional block that are
251 acted upon by UvrD. Rifampicin treatment produced a clearer response, reducing the
252 number of DnaQ foci colocalised with UvrD by ~20% (Figure 3A) and the mean
253 stoichiometry of colocalised and not colocalised UvrD foci by around one UvrD

254 tetramer (Figure 3C and D). Single-molecule observations of RNAP have shown it to
255 be significantly more mobile under rifampicin treatment (95), implying fewer RNAPs
256 bound to DNA and fewer blocks to replication. Our rifampicin treatment results are
257 consistent with fewer transcriptional blocks to replication reducing the amount of UvrD
258 recruited to the replisome and support the hypothesis that UvrD is recruited by these
259 replicative blocks.

260 By deleting *mutS* or *uvrA* we removed UvrD's role in mismatch repair and
261 nucleotide excision repair respectively. Deleting *mutS* surprisingly resulted in no
262 change in UvrD colocalisation with DnaQ but did increase the mean UvrD
263 stoichiometry colocalised with DnaQ by around one tetramer (Figure 3A). In the Δ*uvrA*
264 mutant this resulted in a clear drop of ~25% in UvrD colocalisation with DnaQ (Figure
265 3B) with no change in the number of UvrD foci (Supplementary Figure S8), consistent
266 with the hypothesis that UvrD association with the fork is dependent on actively
267 resolving DNA damage induced blocks to replication. The minimal response in the
268 Δ*mutS* strain may also suggest that UvrD at the fork is more involved in nucleotide
269 excision repair than mismatch repair.

270 UvrD has been shown to compensate for Rep in *rep* null mutants (12). We also
271 tested what effect this mutation would have in our single-molecule assay. Surprisingly,
272 *rep* deletion resulted in a steep drop in UvrD copy number (Supplementary Figure
273 S10). The degree of colocalisation between UvrD and DnaQ remained unchanged
274 compared to wild type (Figure 3A and B) but the stoichiometry of foci was reduced to
275 a single UvrD tetramer (Figure 3C and D and Supplementary Figure 11), presumably
276 due to the lower copy number and availability of UvrD. The drop in UvrD copy number
277 may reflect complex regulatory shifts in response to losing such a key protein in Rep,
278 although it is interesting that even at low copy numbers, a UvrD tetramer remains
279 recruited to the fork. Double knockouts, deficient in both Rep and UvrD, are lethal (12)
280 so this minimal helicase presence must be the limit required for survival.
281

The dynamic association of UvrD with the replication fork is dependent on repair processing

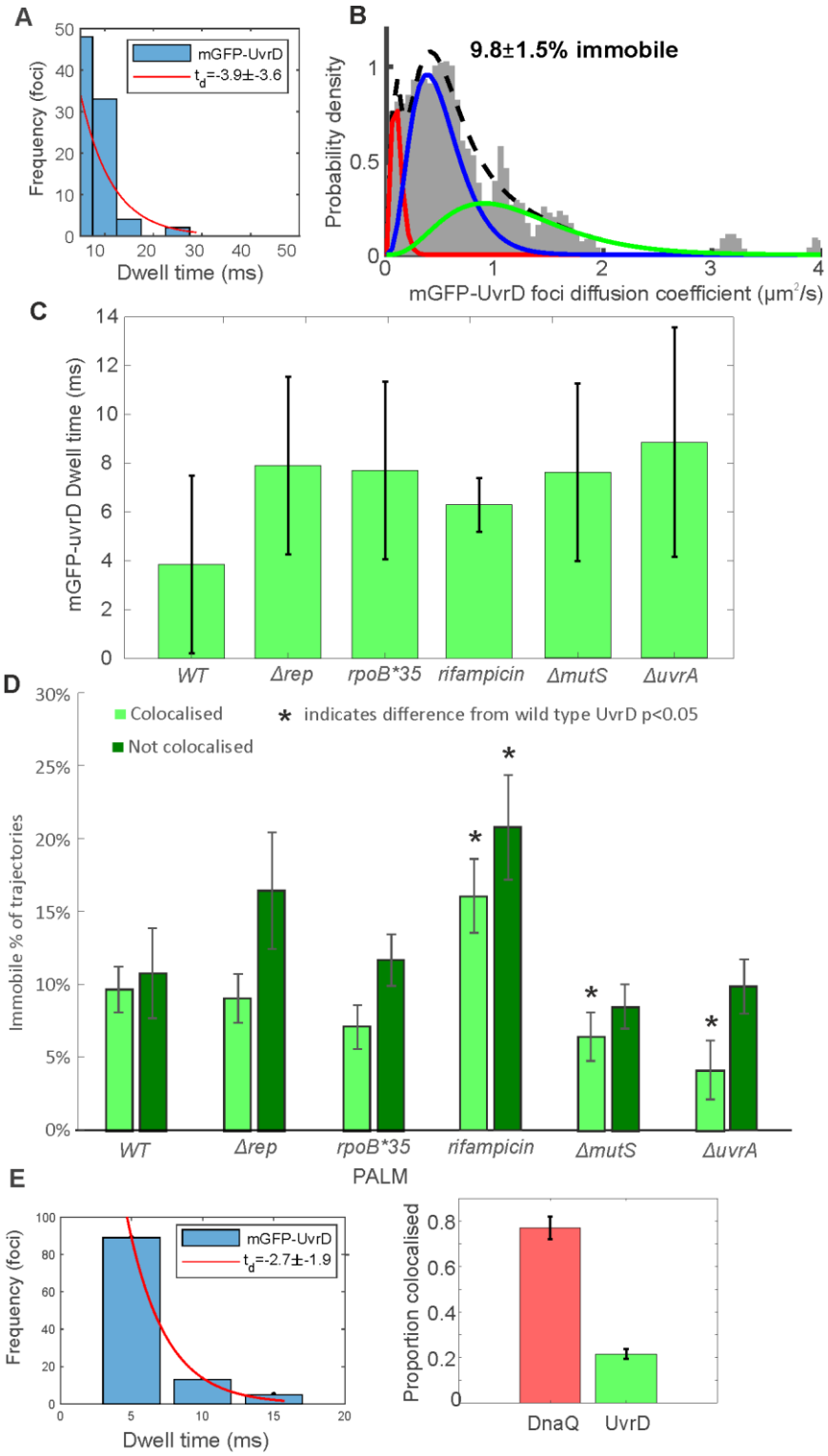

Figure 4: UvrD dynamics. A. Distribution of time over which UvrD and DnaQ foci were colocalised (blue) fitted with an exponential (red) to yield a characteristic dwell time. B. Distribution of microscopic diffusion coefficients of wild type UvrD foci (grey) fitted with a three state gamma distribution model containing a relatively immobile population with $D = 0.1$ μm²/s (red), a transiently immobile population, $D = 0.5$ μm²/s (blue) and a mobile population,

290 D=1.2 μm^2/s (green). C. The dwell times for each UvrD strain. Error bars represent the 95%
291 confidence intervals on the fit. D. The proportion of UvrD foci in the immobile population for
292 each UvrD strain colocalised or not colocalised with DnaQ foci location. Statistically
293 significant differences $p<0.05$ from wild type indicated by *. E. PALM dwell time and
294 colocalisation proportion of detected tracks. N=45 cells for wild type and 30 per mutant, with ~300
295 trajectories.
296

297 By tracking UvrD foci as a function of time using rapid millisecond timescale sampling
298 in Slimfield imaging, we were also able to characterize its dynamics in wild type and
299 repair impaired cells. We measured the number of frames UvrD foci were colocalised
300 with DnaQ foci positions, the dwell time, and calculated the apparent microscopic
301 diffusion coefficient of individual foci (Figure 4 and Supplementary Figure S13). The
302 UvrD dwell time at the fork for the wild type strain was measured to be approximately
303 4 ms, indicating a relatively dynamic association of UvrD at the replication fork. The
304 apparent microscopic diffusion coefficients (*D*) were best fit with a three parameter
305 Gamma model, containing a relatively immobile population with D = 0.1 μm^2/s, a
306 transiently immobile population, D = 0.5 μm^2/s and a mobile population, D=1.2 μm^2/s,
307 similar to Rep (13). In wild type, we found approximately 10% of UvrD foci were
308 immobile, whether colocalised with the DnaQ fork location or not, with the rest of the
309 foci split between the other two populations.

310 We sought to use these molecular measurements to determine the effect of
311 perturbing UvrD-mediated DNA replication repair and block resolution on UvrD
312 dynamics. All deletions resulted in a marginal though statistically negligible increase
313 in dwell time to between 6-9 ms. The Δ*rep* and *rpoB*35* mutations resulted in no
314 change in mobility from wild type. Rifampicin treatment however, resulted in an
315 increase in the proportion of immobile foci both at and away from the fork. This finding
316 appears counterintuitive as rifampicin treatment results in more mobile RNAP (95),
317 however it is unclear what effect rifampicin has on the population of RNAP molecules
318 that remain bound to DNA. These results may suggest that such blocks provide an
319 increased barrier to replication, decreasing mobility of UvrD as it attempts to deal with
320 these blocks. In the Δ*mutS* and Δ*uvrA* strains, the proportion of immobile foci
321 decreased at the fork, again consistent with the hypothesis that UvrD association with
322 the fork is dependent on DNA damage resolution activity. An alternative explanation
323 for these results is that UvrD is less mobile when resolving DNA damage blocks to
324 replication and more mobile when resolving transcriptional blocks, as reducing or

325 eliminating UvrD's role in these processes decreased or increased the immobile
326 fraction in DNA repair and transcription impaired cells respectively (Figure 4).
327
328 ***In vitro* experiments confirm block-dependent UvrD function**
329 To further investigate the role of blocks in UvrD recruitment to the replisome, we
330 performed a stalled replication assay *in vitro,* which allowed us to specifically vary the
331 nucleoprotein block and the timing of UvrD recruitment i.e. before or after the
332 replisome had encountered the block. *E. coli* replisomes can be reconstituted on
333 plasmid DNA templates containing *oriC* and engineered stall sites. UvrD can be
334 included from the start of replication or added after the replisome has encountered the
335 nucleoprotein block. Blocked fork resolution was then probed by examining replication
336 products by denaturing gel electrophoresis.
337 We first used an *oriC*-containing plasmid which contained a specific RNAP stall
338 site ($P_{lacUV5\ 52C}$) to facilitate formation of a stalled transcription elongation complex via
339 nucleotide deprivation. Stalled RNAP acts as a barrier to the replisome in both head-
340 on and co-directional orientations and prevents the formation of full-length replication
341 products (1). Arresting the replisome at this RNAP block resulted in replication
342 products consisting of four truncated leading strands. The strand sizes matched those
343 expected for replisomes moving clockwise or counter-clockwise from *oriC* and
344 encountering $P_{lacUV5\ 52C}$ or the promoters within the *ColE1* plasmid origin of replication
345 (Figure 5A, lane 2 and Figure 5C) (1).
346 Inclusion of UvrD before replication initiation enabled movement of replisomes
347 through stalled RNAP and resulted in a decrease in all four truncated leading strand
348 products and a concomitant increase in production of full-length leading strands
349 (Figure 5A, lane 5 and 5E) (1). Addition of UvrD once the replisome had already
350 encountered the block gave variable results that ranged from an inhibitory to a stronger
351 effect, although differences were not statistically significant at $p<0.05$ (Figure 5A,
352 compare lane 5 with 6, Figure 5E). Similar results were also obtained for Rep (Figure
353 5A, compare lane 3 with 4, Figure 5E). In the absence of replication neither Rep nor
354 UvrD are capable of pushing stalled RNAP from the $P_{lacUV5\ 52C}$ stall site (1). We found
355 that the mGFP tag does not prevent UvrD from dislodging a protein block
356 (Supplementary Figure S14).

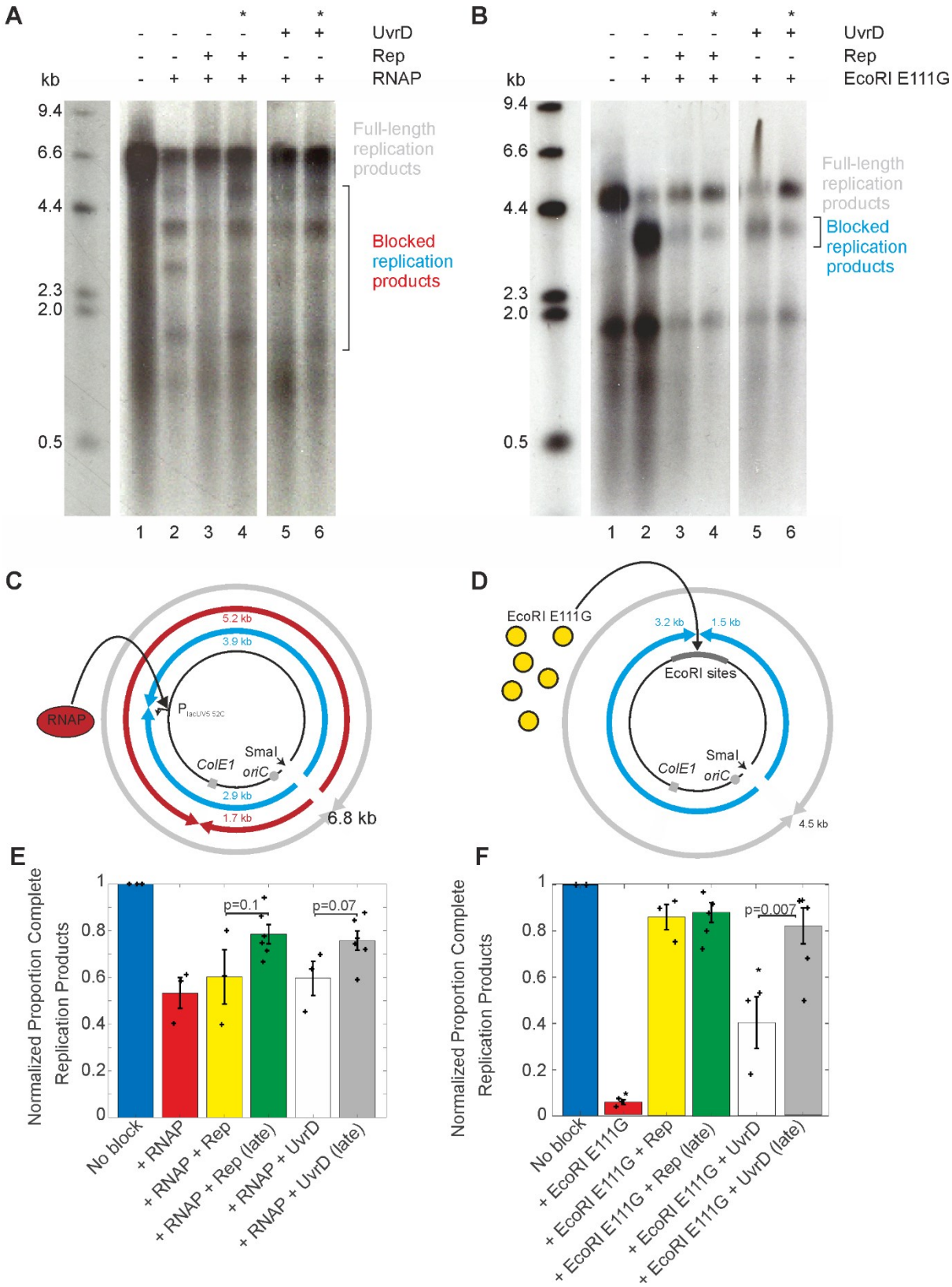

Figure 5: Helicase pre-association affects the promotion of replication fork movement through different nucleoprotein blocks A. Denaturing agarose gel of replication products formed from pPM872 (1) in the absence and presence of RNAP block, Rep and UvrD added pre- and post-collision (*) as indicated. B. Denaturing agarose gel of replication products formed from pPM594 (12) in the absence and presence of EcoRI E111G block, Rep and UvrD added pre- and post-collision (*) as indicated. Truncated leading strand products formed by

364 replisomes originating from *oriC* and colliding with RNAP (C) and EcoRI E111G (D).
365 Quantification of lanes in (A) and (B) from three technical replicates shown in (E) and (F),
366 with standard error in the mean indicated and each replicate result shown as a cross.
367

368 Since UvrD has been shown to interact with RNAP (47–49), we tested whether UvrD-
369 block pre-association is a requirement for its promotion of replication. EcoRI E111G is
370 a mutant restriction enzyme that binds to its recognition sequence but has reduced
371 cleavage activity (96). EcoRI E111G can thus act as an engineered replication fork
372 block that can be overcome by Rep or UvrD helicase activity (12). We tested whether
373 UvrD helicase could promote replication through this barrier when added before or
374 after initiation of replication on a plasmid template with an array of eight EcoRI sites
375 (Figure 5B and D). Adding UvrD post-collision did not impede its promotion of
376 replication; in fact the resolution of these collisions appeared to be more efficient
377 because the proportion of full-length replication products increased (Figure 5B,
378 compare lane 5 and 6, 5F). Quantification of full-length replication products as a
379 proportion of reaction products showed that late UvrD addition increased full-length
380 replication products to 84% (n=6) from 41% (n=3) when UvrD is present before fork
381 collision. This contrasts with the RNAP block results where the UvrD-RNAP interaction
382 (47–50) might be responsible for localising UvrD to the block and facilitating resolution,
383 resulting in no difference when present pre- or post-collision. Similarly, Rep associates
384 directly with the replication fork, also resulting in no difference when present pre- or
385 post-collision, for both blocks. These results suggest that UvrD might recognize stalled
386 replication forks at nucleoprotein blocks using a different mechanism than Rep.
387 Combining these data with the lack of a specific replisome partner and reductions in
388 colocalisation between UvrD and DnaQ fork marker when replication blocks are
389 perturbed *in vivo*, leads us to propose that UvrD is present at the replication fork due
390 to the high frequency of different types of blocks to replication.
391

392 **DISCUSSION**

393 Here, we show that the majority of replisomes are associated with UvrD; but unlike the
394 established Rep association, UvrD has no interaction partner in the replisome. UvrD
395 instead associates with the replisome through the frequent blocks to replication
396 encountered by the fork. Similarly to Rep, *in vitro* evidence suggests UvrD functions
397 poorly as a helicase when monomeric (97). We showed previously that functional Rep
398 foci were hexameric *in vivo* but that this oligomerisation is due to interactions with

399 hexameric DnaB (13). Again, UvrD functions differently and appears to self-associate
400 into tetramers, as evidenced here by tetramer periodicity at and away from the fork
401 (Figure 2 and Supplementary Figure 11) and previous ultracentrifugation experiments
402 *in vitro* (57). It is possible that UvrD may not have evolved to fulfil exactly the same
403 function as Rep. It is common in many enzyme-catalysed reactions that if one enzyme
404 is depleted then another will be available to take its place, but with a reduced catalytic
405 efficiency (98). On initial inspection, this might appear to be the case for Rep and
406 UvrD, in light of the lower efficiency of block resolution for UvrD compared to Rep,
407 noting that deletion of Rep has a profound impact on replication whereas lack of UvrD
408 does not (99). However, we have shown that Rep and UvrD have distinctly different
409 modes of recruitment at a replication block. These differing mechanisms of replication
410 promotion may suggest a model in which these accessory helicases have evolved to
411 fulfil the same overall function (i.e. that of resolving a block to DNA replication) but in
412 different ways. Even with different block removal efficiency, such redundancy may
413 confer an increased level of robustness, helping to ensure that the vital process of
414 DNA replication is carried out correctly by the cell.

415 We used single-molecule microscopy to show that a high proportion of forks,
416 80%, are associated with UvrD *in vivo.* Although the raw imaging data of our Slimfield
417 microscopy is still subject to the optical resolution; the localization tracking algorithms
418 applied can pinpoint fluorescently labelled UvrD to approximately 40 nm lateral
419 precision, smaller than the 50 nm diameter of the replisome machinery itself (69) and
420 equivalent to ~100 bp DNA. Thus, our measurements for colocalisation between UvrD
421 and DnaQ are likely to be good indicators of a real interaction between the replication
422 fork and UvrD. Importantly, the degree of colocalisation we observed is much higher
423 than expectations of random overlap of the optical images of DnaQ-mCherry and
424 mGFP-UvrD.

425 Through SPR, however, we could not find any interaction partner at the
426 replisome apart from Tau. As a control, we tested Tau's interaction with a Rep
427 helicase, and also found a positive interaction. Thus, we conclude that the interaction
428 of UvrD with Tau is likely non-specific and UvrD recruitment to the replisome is
429 mediated by blocks, rather than an interaction partner at the replisome. However, we
430 cannot know the oligomeric state of UvrD on the SPR chip and UvrD's tetrameric form
431 may affect its interactions with replisome components.

432 We probed UvrD's function at the replication fork by perturbing its known DNA
433 repair processing functions, specifically by knocking out *mutS* and *uvrA*, thus blocking
434 mismatch and nucleotide excision repair respectively. We also introduced a mutant
435 RNAP with *rpoB*35* and treated the wild type with rifampicin to reduce the occurrence
436 of transcriptional blocks to translocating replication machinery. Deleting *uvrA* and
437 rifampicin treatment produced clear results, reduced fork colocalization, but deleting
438 *mutS* and introducing the *rpoB*35* mutation did not. However these latter perturbations
439 did result in an identical phenotype of one extra UvrD tetramer per fork. The *rpoB*35*
440 mutation improves cell viability to increased DNA lesions (92). This intriguing link
441 between mutations requires further study, possibly of these dual labelled strains in
442 response to increased DNA lesions. These data support the hypothesis that UvrD is
443 recruited to the replisome by replicative blocks. This is substantiated by the reduced
444 frequency of colocalization observed when mismatch repair and nucleotide excision
445 repair pathways involving UvrD are disrupted. RNA polymerases are the most
446 frequently encountered barrier to replication and we also see a reduction in
447 colocalization when RNA polymerases are removed by the antibiotic.
448 The only function of UvrD we did not probe directly here was its role in RecA-
449 mediated recruitment. We believe the results from a *recA* knockdown would be difficult
450 to interpret due to its pleiotropic effects. RecA is the principal recombinase and
451 induces the complex SOS response resulting in the induction of UvrD expression (100,
452 101). Furthermore, UvrD removes RecA from RecA-DNA complexes, thus functioning
453 as an antirecombinase (102–104). Dissecting these functions of UvrD from other
454 effects that a *recA* mutation may have on the cell would be difficult. Applying the
455 perturbations in combination, i.e. double knockdowns or knockdowns plus rifampicin,
456 would likely lead to confusing results since too many deleterious perturbations may be
457 lethal or change normal cell function too radically to be biologically relevant in the
458 intended way.
459 For the suite of mutant strains investigated we found small but significant
460 changes in colocalisation of UvrD with the replication fork, implying that UvrD is
461 recruited to the replication fork by the frequent blocks to replication it encounters. For
462 example, the UvrD-RNAP interaction could localise UvrD to the vicinity of active
463 transcription machinery (50). Since RNA polymerase is the most common replication
464 block, a secondary consequence would be UvrD-fork colocalisation. This is in contrast
465 to the Rep accessory helicase which has a specific interaction partner in the replisome

466 of the replicative helicase DnaB (89). Recent biochemical findings *in vitro* show that
467 blocks to replication occur very frequently (1)(19)(105), potentially accounting for our
468 finding that UvrD colocalises with the fork more frequently than Rep, despite Rep
469 having a specific interaction partner at the fork.

470 We have shown that replication forks stalled at transcriptional blocks can be
471 rescued by addition of UvrD, prior to or post-stalling. If UvrD is to help perform this
472 function then it must be present during the resolution of collision between the
473 replication and transcription machinery, however, our estimate for dwell time at the
474 fork of just a few milliseconds (compared to seconds for DnaQ (79)) suggests a non-
475 negligible dissociation constant; UvrD is not processive *per se* but rather undergoes
476 rapid turnover at the fork such that there is a high likelihood for UvrD being present at
477 any given time, but not necessarily the same set of molecules. Interestingly we
478 observed a similar dwell time for Rep (13), despite it having a clear association partner
479 in DnaB at the fork. However, using a defective restriction enzyme EcoRI E111G block
480 produced a different effect, with late UvrD addition improving block resolution. This
481 restriction enzyme block is artificial and less biologically relevant but may indicate that
482 the known specific UvrD interaction with RNAP is important. Improved replication
483 resolution with late addition of UvrD is intriguing, implying increased affinity for or
484 activity at pre-stalled replication forks compared to UvrD being present as the fork
485 stalls. Complete understanding requires further study of replication block resolution in
486 different conditions.

487 Our results suggest a model where UvrD diffuses and transiently interacts with
488 DNA at random or through specific interactions such as with RNAP or a specific
489 conformation of the blocked replication fork. At the DNA, UvrD is predominantly
490 tetrameric, either pre-assembling in solution or on the DNA itself. The frequent
491 sampling leads to UvrD often being in the vicinity of the replisome, allowing UvrD to
492 resolve the frequent blocks to replication. It is also possible that certain barriers to
493 replication may be harder for Rep to resolve, and such barriers can possibly be more
494 efficiently removed by UvrD, however, it is still likely to be the case that they do not
495 directly challenge the ability of the cell to replicate the genome in light of *uvrD* deletion
496 still resulting in viable cells. Indeed, UvrD shares a high degree of structural similarity
497 with Rep, although the two proteins differ significantly in their amino acid sequences
498 (31, 106). While Rep is recruited to the fork through specific interactions with DnaB,

499 no such interaction could be identified for UvrD. Stochastic impairment of the ability of
500 Rep to interact with DnaB may necessitate block processing at the fork by UvrD. In
501 summary, our results highlight the contribution of UvrD action to facilitating accurate
502 genome duplication at active replisomes.

503 **Acknowledgments**

504 We thank Maria Chechik for help with mGFP-UvrD purification. We thank Prof. Nigel
505 Savery (University of Bristol) for the gift of the pETDuet-UvrD overexpression plasmid.
506 We thank the Molecular Interactions Laboratory in the Bioscience Technology Facility
507 at the University of York for technical assistance and support. Supported by BBSRC
508 via grants BB/N006453/1 (M.L., P.M.), BB/R001235/1 (M.L.,P.M.), BB/N014863/1
509 (M.H.).

510

511 **Author Contributions**

512 Conceptualization: AJMW, AS, PMG, MH, MCL
513 Methodology: AJMW, AS, JALH, AL, CG, PMG, MH, MCL
514 Software: AJMW
515 Investigation: AJMW, AS, JALH, APD, AL, CG, MH
516 Visualization: AJMW, AS, MH
517 Supervision: AJMW, AS, MH, PMG, MCL
518 Writing—original draft: AJMW, AS, MH, MCL
519 Writing—review & editing: AJMW, AS, JALH, AL, PMG, MH, MCL
520

521 **Declaration of interests**

522 The authors declare no competing interests.
523

524 **MATERIALS AND METHODS**

525 **Strain construction**

526 All strains used in this study (listed in full in SI Table S1, with associated plasmids
527 and primers in SI Tables S2 and S3) are derivatives of the laboratory wild type strain
528 TB28. Tagging of *dnaQ-mCherry-<kan>* (C-terminally labelled) is described in (13).

529 *mGFP-uvrD-<kan>* (N-terminally labelled) was amplified from plasmid pAS79 (*uvrD*$^{+}$)
530 with primers oAS145 and oJGB383 having 50 bp homology to either end of the
531 native *uvrD* locus. The resulting PCR product had homology either side such that
532 recombination with the chromosome would result in integration of the PCR product at
533 the native locus under the control of the native promoter. Prior to integration, all PCR
534 products were treated with DpnI, gel purified, and introduced by electroporation into
535 cells expressing the lambda Red genes from the plasmid pKD46 (55). The
536 recombinants were selected for kanamycin resistance and screened for ampicillin
537 sensitivity. The colonies obtained were verified for integration by PCR and
538 sequencing. The *uvrD* recombinants were verified by PCR amplification using
539 primers oPM319 and oPM320, and sequencing using the primers oJGB417,
540 oJGB418, oPM407, oPM409, oPM411, and oMKG71. Where required, the
541 kanamycin resistance gene was removed by expressing Flp recombinase from the
542 plasmid pCP20 (58) to generate kanamycin sensitive strains carrying the fluorescent
543 protein (FP) fusions. Dual labelled strains were created by introducing the kanamycin
544 tagged FP alleles by standard P1 mediated transduction into single labelled strains
545 carrying the required FP allele after removing the linked kanamycin marker.

546 **Determination of cell doubling time**

547 *E. coli* strains were grown overnight in LB medium at 37°C at 200 rpm shaking. The
548 saturated overnight cultures were diluted 100 fold into fresh LB or washed once with
549 1X 56 salts and diluted 100 fold in fresh 1X 56 salts with 0.2% glucose as the carbon
550 source. Aliquots of 100 µl each of the diluted cultures in fresh media were pipetted
551 into individual wells of 96 well clear flat bottom sterile microplates (Corning). The
552 microplates containing the diluted cultures were incubated in a BMG LABTECH
553 SPECTROstar Nano microplate reader at 37°C and the optical density (A_{600}) values
554 were recorded at defined time intervals. The time taken for the optical density values
555 to increase two fold during the exponential growth phase of the culture was taken as
556 the cell doubling time (SI Table S4, Supplementary Figure S1).

557 **Protein Overexpression and Purification**

558 *mGFP-uvrD* was excised from pAS79 using XhoI and SalI and ligated into pET14b
559 cut with XhoI, creating pAS152 encoding N-terminal histidine-tagged mGFP-UvrD.
560 pAS152 was used to overexpress the mGFP-UvrD fusion in Rosetta™

561 2(DE3)/pLysS. The cells were grown in LB medium containing 100 µg/ml ampicillin
562 and 30 µg/ml chloramphenicol at 37ºC and 220 rpm to OD_{600} ~ 0.7. The cultures
563 were then equilibrated to room temperature and overexpression was induced by
564 adding 1 mM IPTG and incubating at 16ºC for 24 hours. Cells from the expressed
565 culture were collected by centrifugation at 4ºC and frozen at -80ºC. The cells were
566 later thawed on ice and resuspended in buffer A (20 mM Tris-Cl pH 8.3, 500 mM
567 NaCl, 5 mM imidazole, 10% glycerol) along with 0.1 mg/ml lysozyme, 1 mM AEBSF,
568 0.7 µg/ml pepstatin, 0.5 µg/ml leupeptin, 2.5 µg/ml DNase I and 20 µg/ml RNase A
569 and incubated on ice for 30 minutes. Brij-58 was then added to a final concentration
570 of 0.1% v/v and incubated on ice for another 20 minutes. The suspension was
571 sonicated and then clarified by centrifugation at 18,000 rpm for 60 minutes at 4ºC in
572 an SS-34 rotor to remove debris. The lysate containing mGFP-UvrD was applied to a
573 5 ml His-trap FF crude column (GE healthcare) and the protein was purified by
574 chromatography on an imidazole gradient in buffer A. Peak fractions were collected
575 and concentrated using a Vivaspin 500 concentrator (30 kDa MWCO) (Sartorius).
576 Samples were then aliquoted and flash frozen in liquid nitrogen before storage at -
577 80ºC. Protein concentration was determined by Bradford's assay.

578 UvrD was purified as previously described (59). Briefly UvrD was overexpressed in
579 BL21-AI from a pETDuet vector, via induction by IPTG and arabinose. UvrD was
580 purified from the soluble cell extract after lysis through the use of affinity (heparin
581 agarose), anion exchange (Q-sepharose), and gel filtration chromatography. Pure
582 UvrD was then stored at -80ºC after dialysis into storage buffer or used immediately
583 in Size Exclusion Chromatography - Multi-Angle Laser Light Scattering (SEC-
584 MALLS) analysis.

585 Biotinylated UvrD and Rep were purified as previously described (60). Briefly, the
586 proteins were overexpressed in a BL21 (DE3) containing pBirAcm, encoding a biotin
587 ligase via induction by IPTG and the addition of biotin to the growth media. The
588 biotinylated proteins were then purified from the soluble cell extracts by ammonium
589 sulphate precipitation, and affinity chromatography (softlink avidin and heparin
590 agarose). Pure proteins were then dialysed into storage buffer overnight and stored
591 at -80°C

592 **Helicase assay**

593 Assays for unwinding of streptavidin-bound forks were performed using a substrate
594 made by annealing oligonucleotides oPM187B20 (5' end labelled with ^{32}P) and
595 oPM188B34. Reactions were performed in 10 µL volumes containing 40 mM HEPES
596 (pH 8); 10 mM DTT; 10 mM magnesium acetate; 2 mM ATP; 0.1 mg ml^{-1} BSA and
597 1 nM forked DNA substrate. Reactions were carried out as described earlier (13, 61).
598 Briefly, the reaction mixture was pre-incubated at 37°C for five minutes with or
599 without 1 µM streptavidin (Sigma-Aldrich), to which helicase (as indicated) and biotin
600 (Sigma-Aldrich) were added to 100 µM (acting as a trap for free streptavidin) and
601 incubated at 37°C for another 10 minutes. Reactions were stopped by addition of 2.5
602 µl of 2.5% SDS, 200 mM EDTA and 10 mg ml^{-1} of proteinase K. Reactions were then
603 analysed by non-denaturing gel electrophoresis on 10% polyacrylamide TBE gels.
604 The quantification of the unwinding and displacement of streptavidin from the fork
605 was carried out as described in (62).

606 **Preparation of cells for microscopy**

607 Cells were grown overnight in LB to saturation. The overnight cultures were
608 inoculated the next day at 1:1000 dilution in 1X 56 salts supplemented with 0.2%
609 glucose as the carbon source. The dilutions were then grown at 30°C to mid-log
610 phase.

611 **Rifampicin treatment**

612 Cells prepared for microscopy were treated with rifampicin at a final concentration of
613 50 µg/mL for 30 minutes at 30°C.

614 **Microscopy and image analysis**

615 Imaging was performed on a bespoke dual-colour single-molecule microscope (13).
616 Excitation from Obis 488 nm and 561 nm wavelength 50mW lasers (run at 20 mW)
617 was reduced to 10 µm at full width half maximum field in the sample plane producing
618 Slimfield illumination (63) producing a mean excitation intensity of ~0.25 mW/μm^2.
619 Lasers were digitally modulated to 5 ms period to produce alternating laser excitation
620 using National Instruments dynamic I/O module NI 9402. Excitation was coupled into
621 a Zeiss microscope body with the sample mounted on a Mad City Labs nanostage.
622 Images were magnified to 80nm/pixel and imaged using an Andor Ixon 128 emCCD
623 camera. Colour channels were split red/green using a bespoke colour splitter

624 consisting of a dual-pass green/red dichroic mirror centred at long-pass wavelength
625 560 nm and emission filters with 25 nm bandwidths centred at 542 nm and 594 nm.

626 Cells were imaged on agarose pads suffused with minimal media as described
627 previously (64). Foci were detected and tracked using previously described bespoke
628 MATLAB software (65). In brief, bright candidate foci were detected in each frame by
629 image transformation and thresholding based on Otsu's method. A 17x17 pixel
630 region of interest (ROI) is drawn around each candidate to define the local
631 background, while a radius 5 circle is drawn in the center (the foreground) and
632 subjected to iterative Gaussian masking (66). Foci were accepted if their signal to
633 noise ratio was above 0.4, defined as the mean intensity inside the foreground
634 divided by the standard deviation of the local background. Foci in successive frames
635 were linked together into trajectories based on nearest distance, provided it was < 5
636 pixels. Linked foci were accepted as "tracks" nominally if they persist for at least 4
637 consecutive image frames.

638 Characteristic intensity of mGFP or mCherry was determined from the distribution of
639 foci intensity values towards the end of the photobleach confirmed by overtracking
640 foci beyond their bleaching and applying an edge-preserving filter (67, 68) to the raw
641 intensity data to generate individual steps of the characteristic intensity, due to
642 photobleaching (Supplementary Figure S7). This intensity was used to determine the
643 stoichiometry of foci by fitting the first 3 intensity points with a straight line and
644 dividing the intercept by this characteristic intensity. The number of peaks in the
645 Gaussian fits to UvrD was set by running a peak fitting algorithm over the wild type
646 distribution. This number of Gaussians was then used for mutant distributions unless
647 two or more of the Gaussians converged on the same/similar peak value, in which
648 case they were removed. For DnaQ, two peaks were fit as used previously (69).

649 GFP and mCherry images were aligned based on the peak of the 2D cross
650 correlation between their respective brightfield images. Colocalisation between foci
651 and the probability of random colocalisation was determined as described previously
652 (70, 71).

653 The microscopic apparent diffusion coefficients (*D*) were determined by fitting a
654 straight line to the first three mean squared displacements (MSD) values constrained
655 through the equivalent localization precision MSD as determined from the intensity

656 (72, 73). *D* distributions were fit by three Gamma distributions as described
657 previously (74–76). Dwell time was calculated as the number of frames that each
658 trajectory was colocalised with the fork position, as determined by the DnaQ foci
659 detected at time zero.

660 **SEC-MALLS**

661 Size Exclusion Chromatography – Multi-Angle Laser Light Scattering (SEC-MALLS)
662 experiments used Wyatt HELEOS-II multi-angle light scattering and rEX refractive
663 index detectors linked to a Shimadzu HPLC system (SPD-20A UV detector, LC20-
664 AD isocratic pump system, DGU-20A3 degasser and SIL-20A autosampler) with a
665 G.E. Superdex S200 10/300 column at a flow rate of 0.5 mL/min in buffer of 20 mM
666 Tris pH 8.3 (at 4degC) 1 mM EDTA, 1 mm EGTA, 1 mM DTT, 200 mM NaCl, 5%
667 glycerol buffer. Data were analysed using Wyatt Astra 7 software. MWs were
668 estimated using the Zimm fit method with degree 1. A value of 0.182 mL/g was used
669 for protein refractive index increment (dn/dc).

670 **Surface plasmon resonance (SPR)**

671 SPR was performed at 25°C on a BIAcore T200 instrument as in (12). Immobilisation
672 of *E. coli* UvrD and Rep was performed onto streptavidin-coated SA sensor chips
673 whilst the indicated concentrations of Tau and UvrB were passed over in 10 mM
674 HEPES pH 7.4, 3 mM EDTA, 150 mM NaCl, 10 mM $MgCl_2$ and 0.05% Tween 20 at
675 20 µl min^{-1}. This buffer differed from that used in the DNA replication assays to
676 minimise non-specific interactions with the surface-immobilised streptavidin.

677 **Replication assay**

678 Replication assays were carried out using pPM872 as the template for RNAP blocks
679 (1) or pPM594 (12) for EcoRI E111G blocks. Plasmid pPM872 contains $P_{lacUV5\ 52C}$, a
680 strong promoter in which the first 52 nucleotides of the transcript lack cytosine
681 residues and are then followed by four consecutive cytosines. This enables
682 transcription of $P_{lacUV5\ 52C}$ to be stalled by the omission of CTP. Assays were
683 performed in 40 mM HEPES (pH 8); 10 mM DTT; 10 mM magnesium acetate; 2 mM
684 ATP; 0.2 mM GTP, 0.2 mM UTP; 0.04 mM dNTPs; and 0.1 mg/ml BSA. Reactions
685 (15 µl) contained 2 nM plasmid template, 50 nM DNA polymerase III αεθ complex,
686 25 nM τ clamp loader complex, 160 nM DnaB and DnaC monomers, 1 µM SSB, 80

687 nM β clamp, 30 nM HU, 200 nM DnaG, 300 nM DnaA. Helicases were added as
688 indicated. Rep and UvrD used at 200 nM. *E. coli* RNAP holoenzyme from NEB (1
689 U/µl) was used at 1/3 dilution. Dilution was determined empirically to match RNAP
690 replication inhibition levels from (1). EcoRI E111G was purified as in (77) and used
691 at 200 nM. Reactions were assembled on ice and initiated by addition of DnaA and
692 incubation for 4 min at 37°C, followed by addition of 60 units SmaI (Promega) plus
693 0.4 MBq [α^{32}P] dCTP (222 TBq/mmol). Standard reactions with the helicase present
694 in the initial protein mix were carried out at 37°C for 1 minute and then terminated by
695 addition of 1 µl of 0.5 M EDTA. Delayed helicase addition was carried out by adding
696 Rep/UvrD after 1 minute and incubation for a further minute at 37°C before
697 termination with EDTA. Ethanol precipitated replication products were analysed by
698 denaturing agarose gel electrophoresis (0.7% agarose in 2 mM EDTA, 30 mM NaOH
699 for 400 volt hours, standard run was 16 hours at 25 V), phosphorimaging and
700 autoradiography. 5'-labelled HindIII- digested lambda DNA was used as a marker.
701 Gels were quantified using Quantity One® (Bio-Rad) software. Full-length plasmid
702 replication products were quantified as a proportion of summed blocked products
703 and normalised for length (for EcoRI E111G block), or total lane signal (RNAP
704 block).

705

706
707

708

709

710 **REFERENCES**
711

712 1. M. Hawkins, *et al.*, Direct removal of RNA polymerase barriers to replication by
713 accessory replicative helicases. *Nucleic Acids Res.* **47** (2019).
714 2. R. T. Pomerantz, M. O'Donnell, The replisome uses mRNA as a primer after
715 colliding with RNA polymerase. *Nature* **456**, 762–767 (2008).
716 3. H. Merrikh, C. Machón, W. H. Grainger, A. D. Grossman, P. Soultanas, Co-
717 directional replication-transcription conflicts lead to replication restart. *Nature*
718 **470**, 554–7 (2011).
719 4. A. H. Syeda, J. Atkinson, R. G. Lloyd, P. McGlynn, The balance between
720 recombination enzymes and accessory replicative helicases in facilitating
721 genome duplication. *Genes (Basel).* **7** (2016).
722 5. A. Helmrich, M. Ballarino, L. Tora, Collisions between replication and
723 transcription complexes cause common fragile site instability at the longest
724 human genes. *Mol. Cell* **44**, 966–977 (2011).
725 6. Y. Takeuchi, T. Horiuchi, T. Kobayashi, Transcription-dependent
726 recombination and the role of fork collision in yeast rDNA. *Genes Dev.* **17**,
727 1497–1506 (2003).
728 7. A. L. de Septenville, S. Duigou, H. Boubakri, B. Michel, Replication fork
729 reversal after replication-transcription collision. *PLoS Genet.* **8** (2012).
730 8. C. J. Rudolph, A. L. Upton, A. Stockum, C. A. Nieduszynski, R. G. Lloyd,
731 Avoiding chromosome pathology when replication forks collide. *Nature* **500**,
732 608–611 (2013).
733 9. B. Michel, G. Grompone, M. J. Florès, V. Bidnenko, Multiple pathways process
734 stalled replication forks. *Proc. Natl. Acad. Sci. U. S. A.* **101**, 12783–12788
735 (2004).
736 10. E. V. Mirkin, S. M. Mirkin, Mechanisms of transcription-replication collisions in
737 bacteria. *Mol. Cell. Biol.* **25**, 888–895 (2005).
738 11. P. McGlynn, N. J. Savery, M. S. Dillingham, The conflict between DNA
739 replication and transcription. *Mol. Microbiol.* **85**, 12–20 (2012).
740 12. C. P. Guy, *et al.*, Rep provides a second motor at the replisome to promote
741 duplication of protein-bound DNA. *Mol. Cell* **36**, 654–666 (2009).
742 13. A. H. Syeda, *et al.*, Single-molecule live cell imaging of Rep reveals the
743 dynamic interplay between an accessory replicative helicase and the
744 replisome. *Nucleic Acids Res.* **47**, 6287–6298 (2019).
745 14. P. McGlynn, Linking transcription with DNA repair, damage tolerance, and
746 genome duplication. *Proc. Natl. Acad. Sci. U. S. A.* **107**, 15314–15315 (2010).
747 15. D. Dutta, K. Shatalin, V. Epshtein, M. E. Gottesman, E. Nudler, Linking RNA
748 polymerase backtracking to genome instability in E. coli. *Cell* **146**, 533–543
749 (2011).
750 16. D. Duchi, *et al.*, RNA Polymerase Pausing during Initial Transcription. *Mol. Cell*
751 **63**, 939–950 (2016).
752 17. G. Ghosal, J. Chen, DNA damage tolerance: a double-edged sword guarding
753 the genome. *Transl. Cancer Res.* **2**, 107–129 (2013).
754 18. S. Hamperl, M. J. Bocek, J. C. Saldivar, T. Swigut, K. A. Cimprich,
755 Transcription-Replication Conflict Orientation Modulates R-Loop Levels and
756 Activates Distinct DNA Damage Responses. *Cell* **170**, 774-786.e19 (2017).
757 19. K. Hizume, H. Araki, Replication fork pausing at protein barriers on
758 chromosomes. *FEBS Lett.* **593**, 1449–1458 (2019).
759 20. K. K. Myka, M. E. Gottesman, DksA and DNA double-strand break repair.

760 *Curr. Genet.* **65**, 1297–1300 (2019).
761 21. K. K. Myka, *et al.*, Inhibiting translation elongation can aid genome duplication
762 in Escherichia coli. *Nucleic Acids Res.* **45**, 2571–2584 (2017).
763 22. S. M. Mangiameli, C. N. Merrikh, P. A. Wiggins, H. Merrikh, Transcription leads
764 to pervasive replisome instability in bacteria. *Elife* **6** (2017).
765 23. V. Kamarthapu, *et al.*, ppGpp couples transcription to DNA repair in E. coli.
766 *Science* **352**, 993–996 (2016).
767 24. B. J. Brewer, When polymerases collide: replication and the transcriptional
768 organization of the E. coli chromosome. *Cell* **53**, 679–686 (1988).
769 25. A. Srivatsan, A. Tehranchi, D. M. MacAlpine, J. D. Wang, Co-orientation of
770 replication and transcription preserves genome integrity. *PLoS Genet.* **6**
771 (2010).
772 26. B. Liu, B. M. Alberts, Head-on collision between a DNA replication apparatus
773 and RNA polymerase transcription complex. *Science* **267**, 1131–1137 (1995).
774 27. J. D. Wang, M. B. Berkmen, A. D. Grossman, Genome-wide coorientation of
775 replication and transcription reduces adverse effects on replication in Bacillus
776 subtilis. *Proc. Natl. Acad. Sci. U. S. A.* **104**, 5608–5613 (2007).
777 28. T. S. Sankar, B. D. Wastuwidyaningtyas, Y. Dong, S. A. Lewis, J. D. Wang,
778 The nature of mutations induced by replication–transcription collisions. *Nature*
779 **535**, 178–181 (2016).
780 29. D. Ivanova, *et al.*, Shaping the landscape of the Escherichia coli chromosome:
781 replication-transcription encounters in cells with an ectopic replication origin.
782 *Nucleic Acids Res.* **43**, 7865–7877 (2015).
783 30. A. Helmrich, M. Ballarino, E. Nudler, L. Tora, Transcription-replication
784 encounters, consequences and genomic instability. *Nat. Struct. Mol. Biol.* **20**,
785 412–418 (2013).
786 31. J. G. Brüning, J. L. Howard, P. McGlynn, Accessory replicative helicases and
787 the replication of protein-bound DNA. *J. Mol. Biol.* **426**, 3917–3928 (2014).
788 32. K. R. McDonald, *et al.*, Pfh1 Is an Accessory Replicative Helicase that
789 Interacts with the Replisome to Facilitate Fork Progression and Preserve
790 Genome Integrity. *PLoS Genet.* **12** (2016).
791 33. J. E. Sokoloski, A. G. Kozlov, R. Galletto, T. M. Lohman, Chemo-mechanical
792 pushing of proteins along single-stranded DNA. *Proc. Natl. Acad. Sci. U. S. A.*
793 **113**, 6194–6199 (2016).
794 34. G. D. Schauer, *et al.*, Replisome bypass of a protein-based R-loop block by
795 Pif1. *Proc. Natl. Acad. Sci. U. S. A.* **117**, 30354–30361 (2020).
796 35. M. K. Gupta, *et al.*, Protein-DNA complexes are the primary sources of
797 replication fork pausing in Escherichia coli. *Proc. Natl. Acad. Sci. U. S. A.* **110**,
798 7252–7257 (2013).
799 36. H. Boubakri, A. L. De Septenville, E. Viguera, B. Michel, The helicases DinG,
800 Rep and UvrD cooperate to promote replication across transcription units in
801 vivo. *EMBO J.* **29**, 145–157 (2010).
802 37. X. Liu, J. X. Seet, Y. Shi, P. R. Bianco, Rep and UvrD Antagonize One Another
803 at Stalled Replication Forks and This Is Exacerbated by SSB. *ACS Omega* **4**,
804 5180–5196 (2019).
805 38. O. Adebali, Y. Y. Chiou, J. Hu, A. Sancar, C. P. Selby, Genome-wide
806 transcription-coupled repair in Escherichia coli is mediated by the Mfd
807 translocase. *Proc. Natl. Acad. Sci. U. S. A.* **114**, E2116–E2125 (2017).
808 39. N. Kang, E. Choi, S. G. Kim, J. Hwang, Inhibitory effect of UvrD and DinG on
809 the replication of ColE1-derived plasmids in Escherichia coli. *Plasmid* **81**, 32–

810 41 (2015).
811 40. V. Epshtein, UvrD helicase: an old dog with a new trick: how one step
812 backward leads to many steps forward. *Bioessays* **37**, 12–19 (2015).
813 41. P. R. Caron, S. R. Kushner, L. Grossman, Involvement of helicase II (uvrD
814 gene product) and DNA polymerase I in excision mediated by the uvrABC
815 protein complex. *Proc. Natl. Acad. Sci. U. S. A.* **82**, 4925–4929 (1985).
816 42. B. Van Houten. Nucleotide excision repair in Escherichia coli. *Microbiol. Rev.*
817 **54**, 18–51 (1990).
818 43. A. L. Lu, S. Clark, P. Modrich, Methyl-directed repair of DNA base-pair
819 mismatches in vitro. *Proc. Natl. Acad. Sci. U. S. A.* **80**, 4639–4643 (1983).
820 44. S. W. Matson, A. B. Robertson, The UvrD helicase and its modulation by the
821 mismatch repair protein MutL. *Nucleic Acids Res.* **34**, 4089–4097 (2006).
822 45. L. Manelyte, *et al.*, The unstructured C-terminal extension of UvrD interacts
823 with UvrB, but is dispensable for nucleotide excision repair. *DNA Repair*
824 *(Amst).* **8**, 1300–1310 (2009).
825 46. A. B. Robertson, S. R. Pattishall, E. A. Gibbons, S. W. Matson, MutL-catalyzed
826 ATP hydrolysis is required at a post-UvrD loading step in methyl-directed
827 mismatch repair. *J. Biol. Chem.* **281**, 19949–19959 (2006).
828 47. E. J. Gwynn, *et al.*, The conserved C-terminus of the PcrA/UvrD helicase
829 interacts directly with RNA polymerase. *PLoS One* **8** (2013).
830 48. K. Sanders, *et al.*, The structure and function of an RNA polymerase
831 interaction domain in the PcrA/UvrD helicase. *Nucleic Acids Res.* **45**, 3875–
832 3887 (2017).
833 49. V. Epshtein, *et al.*, UvrD facilitates DNA repair by pulling RNA polymerase
834 backwards. *Nature* **505**, 372–377 (2014).
835 50. B. K. Bharati, *et al.*, Crucial role and mechanism of transcription-coupled DNA
836 repair in bacteria. *Nature* **604**, 152–159 (2022).
837 51. B. Martinez, B. K. Bharati, V. Epshtein, E. Nudler, Pervasive Transcription-
838 coupled DNA repair in E. coli. *Nat. Commun.* **13** (2022).
839 52. N. M. Haines, Y. I. T. Kim, A. J. Smith, N. J. Savery, Stalled transcription
840 complexes promote DNA repair at a distance. *Proc. Natl. Acad. Sci. U. S. A.*
841 **111**, 4037–4042 (2014).
842 53. A. J. Smith, N. J. Savery, Effects of the bacterial transcription-repair coupling
843 factor during transcription of DNA containing non-bulky lesions. *DNA Repair*
844 *(Amst).* **7**, 1670–1679 (2008).
845 54. A. J. Smith, N. J. Savery, RNA polymerase mutants defective in the initiation of
846 transcription-coupled DNA repair. *Nucleic Acids Res.* **33**, 755–764 (2005).
847 55. J. Atkinson, *et al.*, Stimulation of UvrD helicase by UvrAB. *J. Biol. Chem.* **284**,
848 9612–9623 (2009).
849 56. R. P. Wong, N. García-Rodríguez, N. Zilio, M. Hanulová, H. D. Ulrich,
850 Processing of DNA Polymerase-Blocking Lesions during Genome Replication
851 Is Spatially and Temporally Segregated from Replication Forks. *Mol. Cell* **77**,
852 3-16.e4 (2020).
853 57. N. K. Maluf, T. M. Lohman, Self-association equilibria of Escherichia coli UvrD
854 helicase studied by analytical ultracentrifugation. *J. Mol. Biol.* **325**, 889–912
855 (2003).
856 58. K. A. Datsenko, B. L. Wanner, One-step inactivation of chromosomal genes in
857 Escherichia coli K-12 using PCR products. *Proc. Natl. Acad. Sci. U. S. A.* **97**,
858 6640–6645 (2000).
859 59. J. Atkinson, *et al.*, Stimulation of UvrD helicase by UvrAB. *J. Biol. Chem.* **284**,

860 9612–9623 (2009).
861 60. C. P. Guy, *et al.*, Rep provides a second motor at the replisome to promote
862 duplication of protein-bound DNA. *Mol. Cell* **36**, 654–666 (2009).
863 61. J. G. Brüning, J. A. L. Howard, K. K. Myka, M. S. Dillingham, P. McGlynn, The
864 2B subdomain of Rep helicase links translocation along DNA with protein
865 displacement. *Nucleic Acids Res.* **46**, 8917–8925 (2018).
866 62. J. G. Brüning, J. A. L. Howard, P. McGlynn, Use of streptavidin bound to
867 biotinylated DNA structures as model substrates for analysis of nucleoprotein
868 complex disruption by helicases. *Methods* **108**, 48–55 (2016).
869 63. M. Plank, G. H. Wadhams, M. C. Leake, Millisecond timescale slimfield
870 imaging and automated quantification of single fluorescent protein molecules
871 for use in probing complex biological processes. *Integr. Biol.* **1**, 602–612
872 (2009).
873 64. A. J. M. Wollman, A. H. Syeda, P. McGlynn, M. C. Leake, Single-Molecule
874 Observation of DNA Replication Repair Pathways in E. coli. *Adv. Exp. Med.*
875 *Biol.* **915**, 5–16 (2016).
876 65. H. Miller, *et al.*, Superresolution imaging of single DNA molecules using
877 stochastic photoblinking of minor groove and intercalating dyes. *Methods* **88**,
878 81–8 (2015).
879 66. M. C. Leake, *et al.*, Stoichiometry and turnover in single, functioning
880 membrane protein complexes. *Nature* **443**, 355–358 (2006).
881 67. M. C. Leake, D. Wilson, B. Bullard, R. M. Simmons, The elasticity of single
882 kettin molecules using a two-bead laser-tweezers assay. *FEBS Lett.* **535**, 55–
883 60 (2003).
884 68. M. C. Leake, D. Wilson, M. Gautel, R. M. Simmons, The elasticity of single titin
885 molecules using a two-bead optical tweezers assay. *Biophys. J.* **87**, 1112–35
886 (2004).
887 69. R. Reyes-Lamothe, D. J. Sherratt, M. C. Leake, Stoichiometry and architecture
888 of active DNA replication machinery in Escherichia coli. *Science* **328**, 498–501
889 (2010).
890 70. I. Llorente-Garcia, *et al.*, Single-molecule in vivo imaging of bacterial
891 respiratory complexes indicates delocalized oxidative phosphorylation.
892 *Biochim. Biophys. Acta* **1837**, 811–24 (2014).
893 71. A. J. M. Wollman, *et al.*, Critical roles for EGFR and EGFR-HER2 clusters in
894 EGF binding of SW620 human carcinoma cells. *J. R. Soc. Interface* **19** (2022).
895 72. A. J. M. Wollman, M. C. Leake, Millisecond single-molecule localization
896 microscopy combined with convolution analysis and automated image
897 segmentation to determine protein concentrations in complexly structured,
898 functional cells, one cell at a time. *Faraday Discuss.* **184**, 401–24 (2015).
899 73. M. C. Leake, *et al.*, Variable stoichiometry of the TatA component of the twin-
900 arginine protein transport system observed by in vivo single-molecule imaging.
901 *Proc. Natl. Acad. Sci. U. S. A.* **105**, 15376–81 (2008).
902 74. H. Miller, *et al.*, High-Speed Single-Molecule Tracking of CXCL13 in the B-
903 Follicle. *Front. Immunol.* **9**, 1073 (2018).
904 75. J. Cosgrove, *et al.*, B cell zone reticular cell microenvironments shape CXCL13
905 gradient formation. *Nat. Commun.* **11** (2020).
906 76. X. Jin, *et al.*, Membraneless organelles formed by liquid-liquid phase
907 separation increase bacterial fitness. *Sci. Adv.* **7** (2021).
908 77. S.-C. Chengs, R. Kim, K. Kings, S.-H. Kim, P. Modrich, Isolation of Gram
909 Quantities of EcoRI Restriction and Modification Enzymes from an

910 Overproducing Strain. *J. Biol. Chem.* **259**, 11571–11575 (1984).
911 78. A. Badrinarayanan, R. Reyes-Lamothe, S. Uphoff, M. C. Leake, D. J. Sherratt,
912 In vivo architecture and action of bacterial structural maintenance of
913 chromosome proteins. *Science* **338**, 528–31 (2012).
914 79. T. R. Beattie, *et al.*, Frequent exchange of the DNA polymerase during
915 bacterial chromosome replication. *Elife* **6**, e21763 (2017).
916 80. R. Reyes-Lamothe, C. Possoz, O. Danilova, D. J. Sherratt, Independent
917 positioning and action of Escherichia coli replisomes in live cells. *Cell* **133**, 90–
918 102 (2008).
919 81. A. L. Payne-Dwyer, A. H. Syeda, J. W. Shepherd, L. Frame, M. C. Leake,
920 RecA and RecB: probing complexes of DNA repair proteins with mitomycin C
921 in live Escherichia coli with single-molecule sensitivity. *bioRxiv*,
922 2021.10.04.463068 (2021).
923 82. D. A. Zacharias, J. D. Violin, A. C. Newton, R. Y. Tsien, Partitioning of lipid-
924 modified monomeric GFPs into membrane microdomains of live cells. *Science*
925 **296**, 913–916 (2002).
926 83. N. K. Maluf, C. J. Fischer, T. M. Lohman, A Dimer of Escherichia coli UvrD is
927 the active form of the helicase in vitro. *J. Mol. Biol.* **325**, 913–935 (2003).
928 84. H. Yokota, Y. A. Chujo, Y. Harada, Single-molecule imaging of the oligomer
929 formation of the nonhexameric Escherichia coli UvrD helicase. *Biophys. J.* **104**,
930 924–933 (2013).
931 85. H. Yokota, Quantitative and kinetic single-molecule analysis of DNA unwinding
932 by Escherichia coli UvrD helicase. *Biophys. physicobiology* **19**, n/a (2022).
933 86. H. M. Arthur, P. B. Eastlake, Transcriptional control of the uvrD gene of
934 Escherichia coli. *Gene* **25**, 309–316 (1983).
935 87. Y. Taniguchi, *et al.*, Quantifying E. coli proteome and transcriptome with
936 single-molecule sensitivity in single cells. *Science* **329**, 533–8 (2010).
937 88. G. W. Li, D. Burkhardt, C. Gross, J. S. Weissman, Quantifying absolute protein
938 synthesis rates reveals principles underlying allocation of cellular resources.
939 *Cell* **157**, 624–635 (2014).
940 89. J. Atkinson, M. K. Gupta, P. McGlynn, Interaction of Rep and DnaB on DNA.
941 *Nucleic Acids Res.* **39**, 1351–1359 (2011).
942 90. S. V. Rajagopala, *et al.*, The binary protein-protein interaction landscape of
943 Escherichia coli. *Nat. Biotechnol. 2014 323* **32**, 285–290 (2014).
944 91. D. K. Orrens, C. P. Selbys, J. E. Hearst, A. Sancars, Post-incision Steps of
945 Nucleotide Excision Repair in Escherichia coli DISASSEMBLY OF THE
946 UvrBC-DNA COMPLEX BY HELICASE I1 AND DNA POLYMERASE I*. *J.*
947 *Biol. Chem.* **267**, 780–788 (1992).
948 92. P. McGlynn, R. G. Lloyd, Modulation of RNA polymerase by (p)ppGpp reveals
949 a RecG-dependent mechanism for replication fork progression. *Cell* **101**, 35–
950 45 (2000).
951 93. Y. N. Zhou, D. J. Jin, The rpoB mutants destabilizing initiation complexes at
952 stringently controlled promoters behave like “stringent” RNA polymerases in
953 Escherichia coli. *Proc. Natl. Acad. Sci. U. S. A.* **95**, 2908–2913 (1998).
954 94. E. A. Campbell, *et al.*, Structural mechanism for rifampicin inhibition of
955 bacterial rna polymerase. *Cell* **104**, 901–912 (2001).
956 95. M. Stracy, *et al.*, Live-cell superresolution microscopy reveals the organization
957 of RNA polymerase in the bacterial nucleoid. *Proc. Natl. Acad. Sci. U. S. A.*
958 **112**, E4390-9 (2015).
959 96. K. King, S. J. Benkovics, P. Modrich, Glu-11 1 Is Required for Activation of the

960 DNA Cleavage Center of EcoRI Endonuclease*. *J. Biol. Chem.* **264**, 11807–
961 11815 (1989).
962 97. B. Nguyen, Y. Ordabayev, J. E. Sokoloski, E. Weiland, T. M. Lohman, Large
963 domain movements upon UvrD dimerization and helicase activation. *Proc.*
964 *Natl. Acad. Sci.* **114**, 12178–12183 (2017).
965 98. A. Wagner, Robustness against mutations in genetic networks of yeast. *Nat.*
966 *Genet. 2000 244* **24**, 355–361 (2000).
967 99. J. Atkinson, *et al.*, Localization of an accessory helicase at the replisome is
968 critical in sustaining efficient genome duplication. *Nucleic Acids Res.* **39**, 949–
969 957 (2011).
970 100. S. C. Massoni, S. J. Sandler, Specificity in suppression of SOS expression by
971 recA4162 and uvrD303. *DNA Repair (Amst).* **12**, 1072–1080 (2013).
972 101. K. H. Maslowska, K. Makiela-Dzbenska, I. J. Fijalkowska, The SOS system: A
973 complex and tightly regulated response to DNA damage. *Environ. Mol.*
974 *Mutagen.* **60**, 368–384 (2019).
975 102. R. C. Centore, S. J. Sandler, UvrD limits the number and intensities of RecA-
976 green fluorescent protein structures in Escherichia coli K-12. *J. Bacteriol.* **189**,
977 2915–2920 (2007).
978 103. V. Petrova, *et al.*, Active displacement of RecA filaments by UvrD translocase
979 activity. *Nucleic Acids Res.* **43**, 4133–4149 (2015).
980 104. M. M. Cox, Regulation of bacterial RecA protein function. *Crit. Rev. Biochem.*
981 *Mol. Biol.* **42**, 41–63 (2007).
982 105. N. Raghunathan, S. Goswami, J. K. Leela, A. Pandiyan, J. Gowrishankar, A
983 new role for Escherichia coli Dam DNA methylase in prevention of aberrant
984 chromosomal replication. *Nucleic Acids Res.* **47**, 5698–5711 (2019).
985 106. H. Yokota, Roles of the C-Terminal Amino Acids of Non-Hexameric Helicases:
986 Insights from Escherichia coli UvrD. *Int. J. Mol. Sci.* **22**, 1–19 (2021).
987
988
989

Supplementary Information

Tetrameric UvrD helicase is located at the *E. coli* replisome due to frequent replication blocks

Adam J. M Wollman[1,2,3,], Aisha H. Syeda[1,2], Jamieson A. L. Howard[1,2], Alex Payne-Dwyer[1,2], Andrew Leech[4] , Colin Guy[5, 6], Peter McGlynn[2,6], Michelle Hawkins[2] and Mark C. Leake[1,2]

The authors wish it to be known that, in their opinion, the first two authors should be regarded as joint First Authors

[1] School of Physics, Engineering and Technology, University of York, York YO10 5DD, United Kingdom.

[2] Department of Biology, University of York, York YO10 5DD, United Kingdom.

[3] Current address: Biosciences Institute, Newcastle University, NE1 7RU, United Kingdom.

[4] Bioscience Technology Facility, Department of Biology, University of York, York YO10 5DD, United Kingdom

[5] Current address: Covance Laboratories Ltd., Otley Road, Harrogate, HG3 1PY, United Kingdom

[6] Previous address: School of Medical Sciences, Institute of Medical Sciences, University of Aberdeen, Foresterhill, Aberdeen AB25 2ZD, United Kingdom

* To whom correspondence should be addressed. To whom correspondence should be addressed. Tel: +44 (0)1904322697. Email: mark.leake@york.ac.uk

Present Address: School of Physics, Engineering and Technology, and Department of Biology, University of York, York YO10 5DD, United Kingdom

1014 **Supplementary Tables**

1015 **Table S1 Strains used in this study**

Strain	Relevant genotype	Source or derivation
BW25113 derivatives:		
BW25113	*rrnB ΔlacZ4787 hsdR514 Δ(araBAD)567 Δ(rhaBAD)568 rph-1*	(1)
JW2703	*ΔmutS::<kan>*	(1)
JW3786	*ΔuvrD::<kan>*	(1)
JW4019	*ΔuvrA::<kan>*	(1)
MG1655 derivatives:		
TB12	*ΔlacIZYA::<kan>*	
TB28	*ΔlacIZYA*	(2, 3)
TB28 derivatives		
N6577	*ΔlacIZYA Δrep::cat*	(4)
N6661	*ΔlacIZYA::<> Δrep::dhfr* / pAM407 (*uvrD*$^+$ *lacZ*$^+$, a pRC7 derivative)	(4)
N6661	*ΔlacIZYA::<> Δrep::dhfr* / pAM407 (*uvrD*$^+$ *lacZ*$^+$, a pRC7 derivative)	(4)
N6644	*ΔlacIZYA::<> uvrD::dhfr Δrep::cat* / pAM407 (*uvrD*$^+$ *lacZ*$^+$, a pRC7 derivative)	(4)
JGB166	*ΔuvrD* / pKD46	JW3786 transformed with pKD46
AS97	TB28/pKD46	(5)
AS446	*dnaQ-mCherry-<kan>*	
AS448	*dnaQ-mCherry-<>*	(5)
AS512	*mGFP-uvrD-<kan>*	*mGFP-uvrD-<kan>* recombineered into JGB166
AS517	*ΔlacIZYA::<> Δrep::cat mGFP-uvrD-<kan>* / pAM407 (*uvrD*$^+$ *lacZ*$^+$, a pRC7 derivative)	N6661 X P1(AS512)
AS564	*dnaQ-mCherry-<kan> rpoB*35*	PM486 X P1(AS446)
AS571	*dnaQ-mCherry-<> rpoB*35*	AS564 to km^S with pCP20
AS580	*dnaQ-mCherry-<> mGFP-uvrD-<kan>*	AS448 X P1(AS512)
AS582	*dnaQ-mCherry-<> mGFP-uvrD-<kan> rpoB*35*	AS571 X P1(AS512)
AS590	*dnaQ-mCherry-<> mGFP-uvrD-<kan> Δrep::cat*	AS580 X P1(N6577)
AS650	*dnaQ-mCherry-<> mGFP-uvrD-<>*	AS580 to km^S with pCP20
AS656	*dnaQ-mCherry-<> mGFP-uvrD-<> ΔuvrA::<kan>*	AS650 X P1(JW4019)
AS658	*dnaQ-mCherry-<> mGFP-uvrD-<> ΔmutS::<kan>*	AS650 X P1(JW2703)

1016

1017

1018 **Table S2 Plasmids used in this study**

Plasmid	Description	Antibiotic	Reference
pCP20	Yeast Flp recominase expression plasmid	Amp	(6)
pKD46	λ Red recombinase expression plasmid	Amp	(6)
pAS79	pUC18 *mGFP-uvrD-<kan>*	Amp, kan	This study
pAS152	pET14b-mGFP uvrD	Amp	This study

1019
1020

1021 **Table S3 Oligonucleotides used in this study**

Primer	Sequence (5' - 3')
oJGB383	TGAATGATTTTTTAGGCCAAATAAGGTGCGCAGCACCGCATCCGGCAACGCATATGAATATCCTCCTTAG
oJGB417	TACAAGACACGTGCTGAAGTC
oJGB418	TGCTAGTTGAACGCTTCCATC
oMKG71	CGGTGCCCTGAATGAACTGC
oPM319	CTTGTTGGATCAGACCGGAAAATG
oPM320	TGGCAACGCTATCCTTTTGTCA
oPM407	GCGGCAGGCAATGTGGTA
oPM409	CCTTTGAGCGTGTGGTGA
oPM411	CAGCGGCTACAAGCTCGG
oPM187B20	GTCGGATCCTCTAGACAGC(BiodT)CCATGATCACTGGCACTGGTAGAATTCGGC
oPM188B34	AACGTCATAGACGATTACATTGCTACATGGAGC(BiodT)GTCTAGAGGATCCGAC
oAS84	CCCGTCTCGATCTGGTGCAG
oAS85	TTGCTGCAAAAATCGCCCAAG
oAS132	CCCGTCTCGATCTGGTGCAGAAGAAAGGCGGAAGTTGCCTCTGGCGAGCAGGCTGGCTCCGCTGCTGG
oAS133	TTGCTGCAAAAATCGCCCAAGTCGCTATTTTTAGCGCCTTTCACAGGTATCATATGAATATCCTCCTTAG
oAS145	AGGGCGTTGCGCTTCTCCGCCCAACCTATTTTTACGCGGCGGTGCCAATGAGTAAAGGAGAAGAACTT

1022

1023

1024 **Table S4 Cell doubling times of labelled strains.** Values expressed are the means of three
1025 independent replicates, with standard deviation and standard errors indicated.

Strain (Relevant genotype)	**LB medium**			**Minimal medium**		
	Mean doubling time (min)	**SD (min)**	**SEM (min)**	**Mean doubling time (min)**	**SD (min)**	**SEM (min)**
WT	23.72	1.11	0.64	62.80	17.06	9.85
dnaQ-mCherry	26.85	0.91	0.52	62.22	18.63	10.76
mGFP-uvrD	24.79	0.37	0.22	59.45	1.80	1.04
dnaQ-mCherry mGFP-uvrD	25.27	1.51	0.87	71.03	7.59	4.38
ΔmutS	24.59	0.55	0.32	107.91	13.96	8.06
ΔuvrA	27.99	0.23	0.13	92.25	5.86	3.38
*ΔrpoB*35*	33.98	0.17	0.10	83.11	30.83	17.80
Δrep	24.30	2.03	1.17	62.74	1.20	0.70
dnaQ-mCherry mGFP-uvrD ΔmutS	26.85	0.68	0.39	110.84	34.91	20.16
dnaQ-mCherry mGFP-uvrD ΔuvrA	24.13	0.56	0.33	91.80	5.18	2.99
*dnaQ-mCherry mGFP-uvrD ΔrpoB*35*	32.81	0.70	0.40	99.11	78.68	45.42
dnaQ-mCherry mGFP-uvrD Δrep	26.54	1.90	1.10	62.17	2.98	1.72

1026
1027
1028
1029
1030

1031

1032 **Supplementary figures**

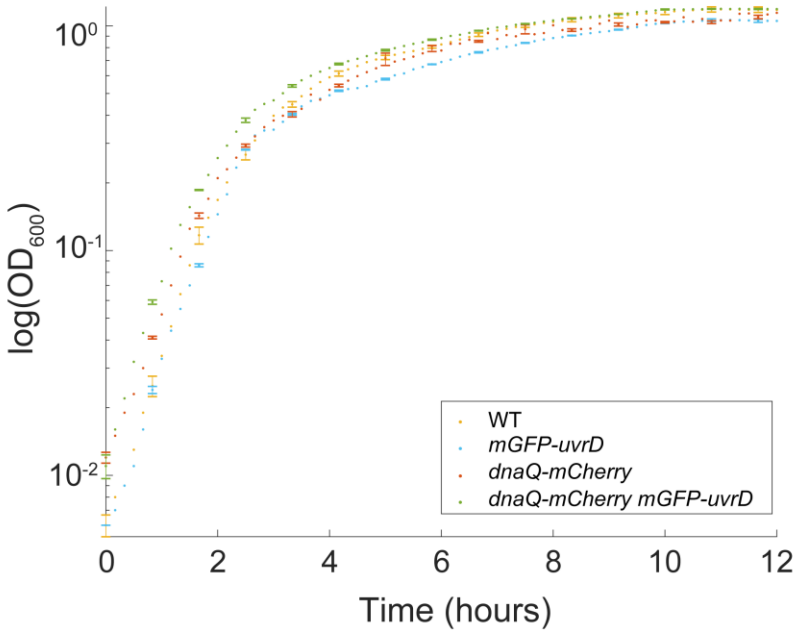

1033

1034

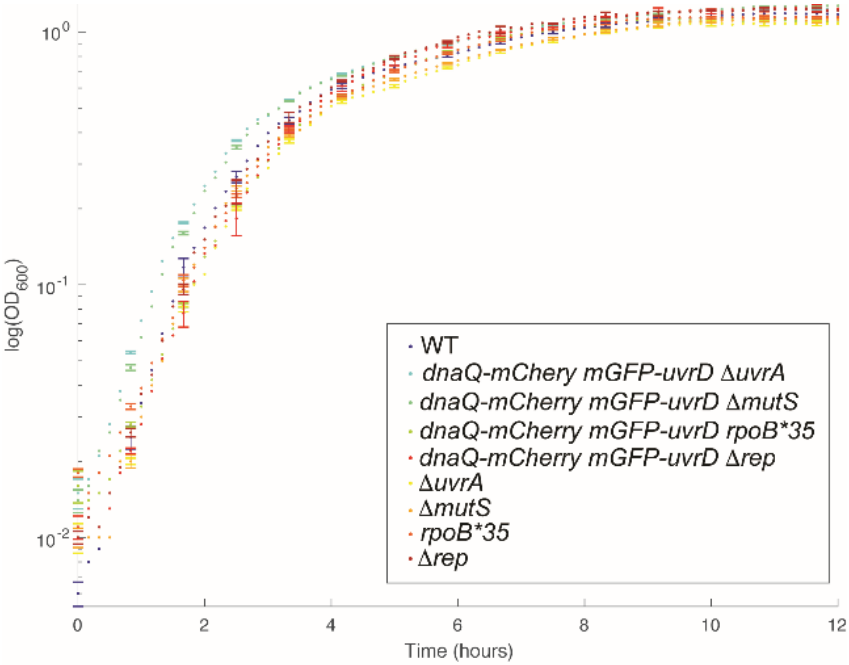

1035

1036 **Supplementary Figure S1. Growth curves in LB medium.** Cultures were grown in LB as
1037 described in the text. The OD_{600} values are plotted on a log scale on the vertical axis with a
1038 linear scale of time in hours on the horizontal axis. The genotypes of the strains are indicated
1039 in boxes within the figures. SD error bars (shown just on every 5th consecutive point for clarity
1040 here), taken from N=3 replicate cultures. Plots in panel A are growth curves of single and dual
1041 labelled wild-type strains, while those in panel B are dual labelled and unlabelled mutant
1042 strains. The unlabelled wild-type strain is included in all panels as a reference.

1043

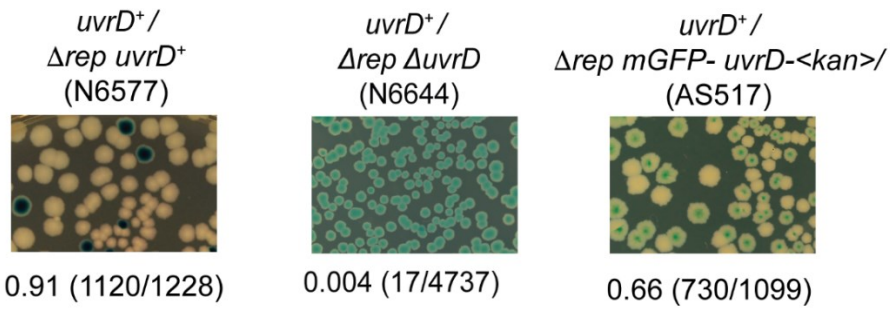

1044

1045 **Supplementary Figure S2: Testing of mGFP-UvrD fusions for retention of function.** We
1046 transformed the strain carrying a chromosomal *mGFP-uvrD* allele with a derivative of pRC7
1047 carrying a wild-type *uvrD* allele (pPM407), which is an unstable low copy plasmid that also
1048 carries the *lacZYA* genes (3). Presence of this plasmid confers blue colour to the colonies on
1049 plates containing Xgal when strains are chromosomally deleted for the *lac* operon. In rapidly
1050 growing cells, cells require either *rep* or *uvrD* for viability, and the loss of both is lethal (4, 7).
1051 Thus, *Δrep* cells with a functional *uvrD* allele are viable and can lose pRC7*uvrD*, evidenced
1052 by appearance of white colonies on LB Xgal IPTG plates, but cells lacking *uvrD* function
1053 cannot survive upon loss of the plasmid resulting in recovery of only blue colonies. The *Δrep*
1054 *mGFP-uvrD* cells produced white colonies on Xgal media, indicating that the *mGFP-uvrD*
1055 fusion is functional.
1056

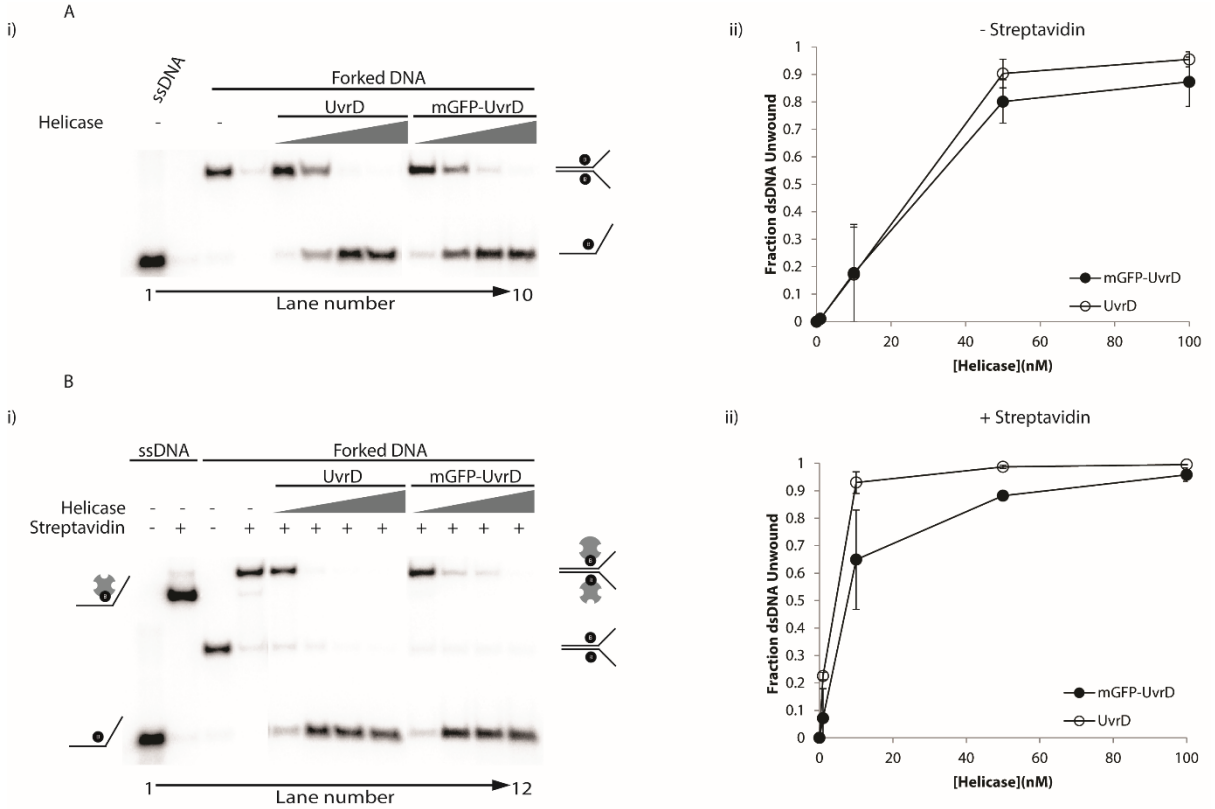

Supplementary Figure S3: mGFP-UvrD fusion is functional *in vitro*. (A)(i) Representative native polyacrylamide TBE gel showing UvrD and mGFP-UvrD unwinding of forked DNA containing biotin on both strands within the duplex region (8, 9). Lanes 1-2 contain markers indicating the position of single stranded or forked DNA as indicated. Lanes 3-10 contain the products of unwinding the forked DNA by the indicated helicase at 1, 10, 50 and 100 nM. (ii) Quantification of the unwinding of the forked substrate by the indicated helicases. Data points shown are averages of band intensities (taken from two gels in UvrD and four gels in mGFP-UvrD) with standard errors indicated by bars on the points. (B)(i) Representative native polyacrylamide TBE gels showing UvrD and mGFP-UvrD unwinding of forked DNA containing biotin on both strands within the duplex region (8, 9). Lanes 1-4 contain markers indicating the position of single stranded or forked DNA +/- streptavidin as indicated. Lanes 5-12 contain the products of unwinding the forked DNA +/- streptavidin by the indicated helicase at 1, 10, 50 and 100 nM. (ii) Quantification of the unwinding of the forked substrate in the presence of streptavidin by the indicated helicases. Data points shown are averages of band intensities (taken from two gels in UvrD and four gels in mGFP-UvrD) with standard errors indicated by bars on the points.

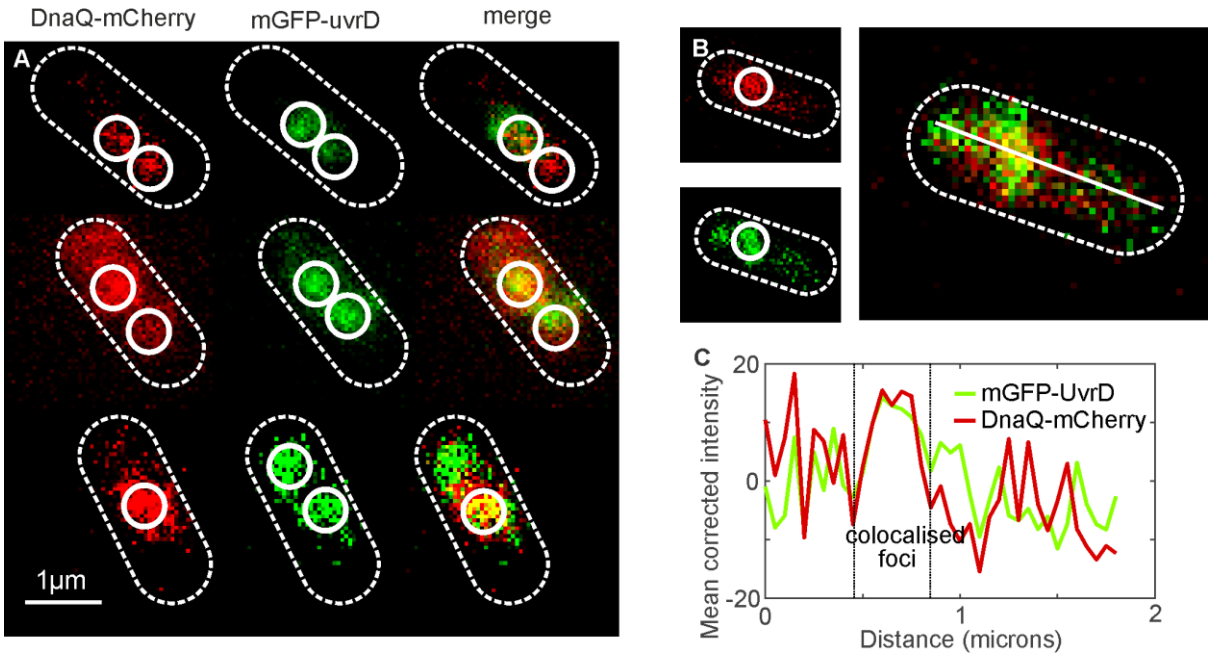

1075

1076 **Supplementary Figure S4: A. and B.** Dual colour Slimfield images of mGFP-UvrD:DnaQ-
1077 mCherry, scale bar 1 micron. Segmented outlines of cell bodies (white dash) and detected
1078 foci (white circles) indicated. C. Mean corrected intensity line profile through a colocalized
1079 foci in B.

1080

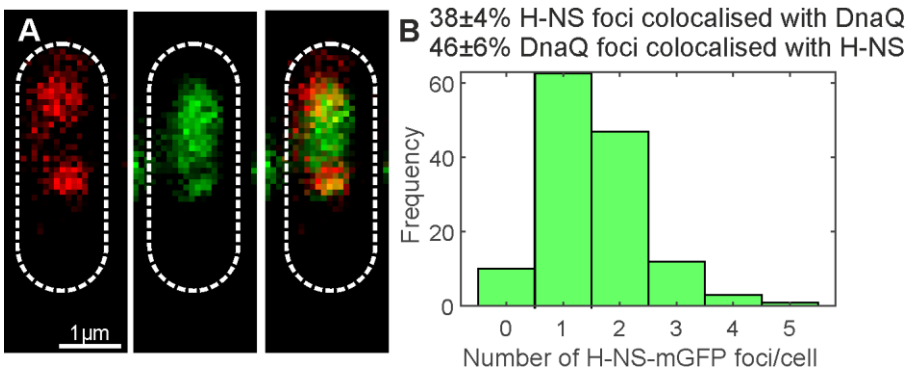

Supplementary Figure S5: (A) Dual colour Slimfield images of H-NS-mGFP-:DnaQ-mCherry, scale bar 1 micron. Segmented outlines of cell bodies indicated (white dash). (B) Histogram showing the number of H-NS foci detected per cell, SD errors.

1086

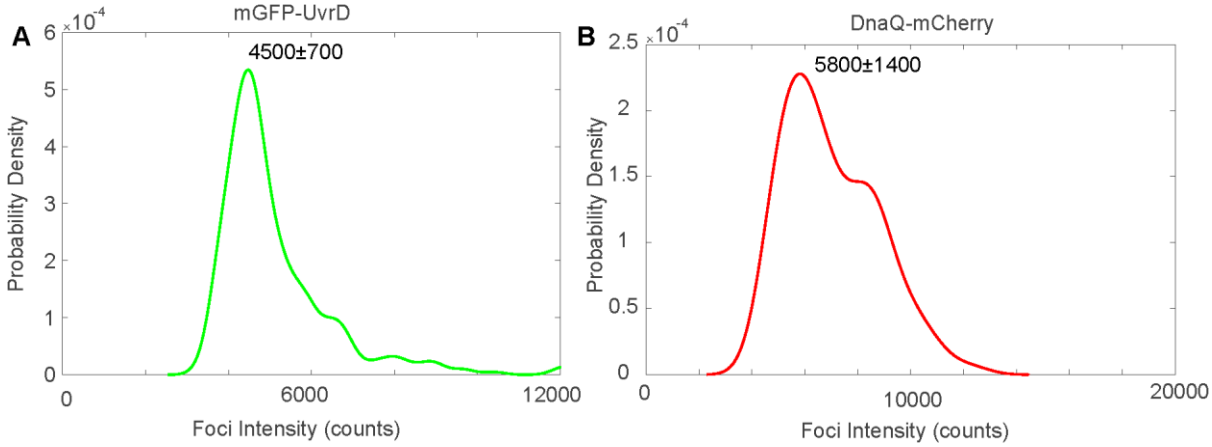

1087

1088 **Supplementary Figure S6: Brightness of single mGFP and mCherry molecules** A. and
1089 B. Characteristic intensity distributions rendered as kernel density estimates of single mGFP-
1090 UvrD and DnaQ-mCherry. Peak±full width at half maximum indicated. Distributions calculated
1091 from the tracked foci intensity distributions from the end of the photobleach process such that
1092 only single fluorophore molecules are detected. Number of molecules per foci before
1093 bleaching is determined by dividing the initial foci intensity by these values for the equivalent
1094 fluorophore.

1095

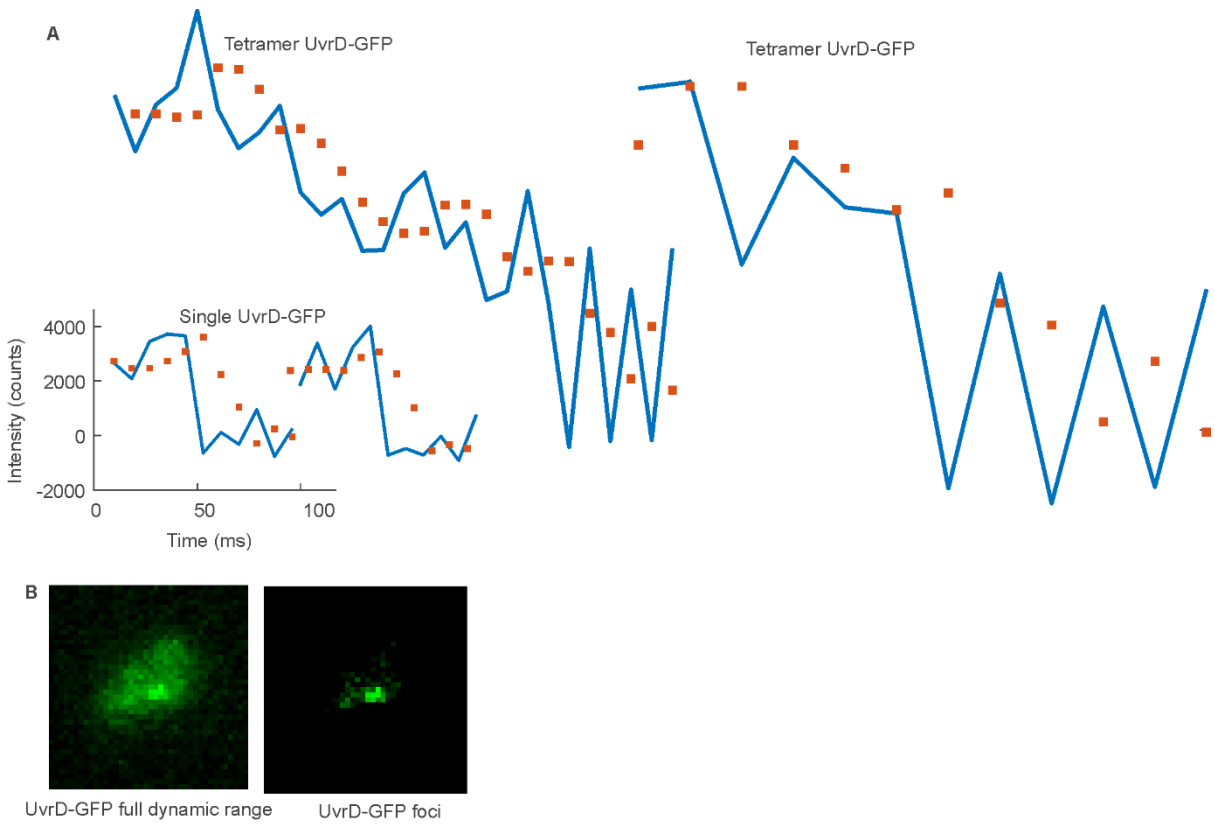

Supplementary Figure S7: Single-molecule image analysis. A. Chung-Kennedy filtered (squares) intensity traces for single UvrD tracks showing tetramers exhibiting multiple photobleach steps and monomers detected towards the end of photobleaching. Foci were 'overtracked' beyond the last detected bright frame to illustrate steps. **B**. UvrD-GFP micrograph showing the full dynamic range (left) and adjusted to illustrate a foci (right)

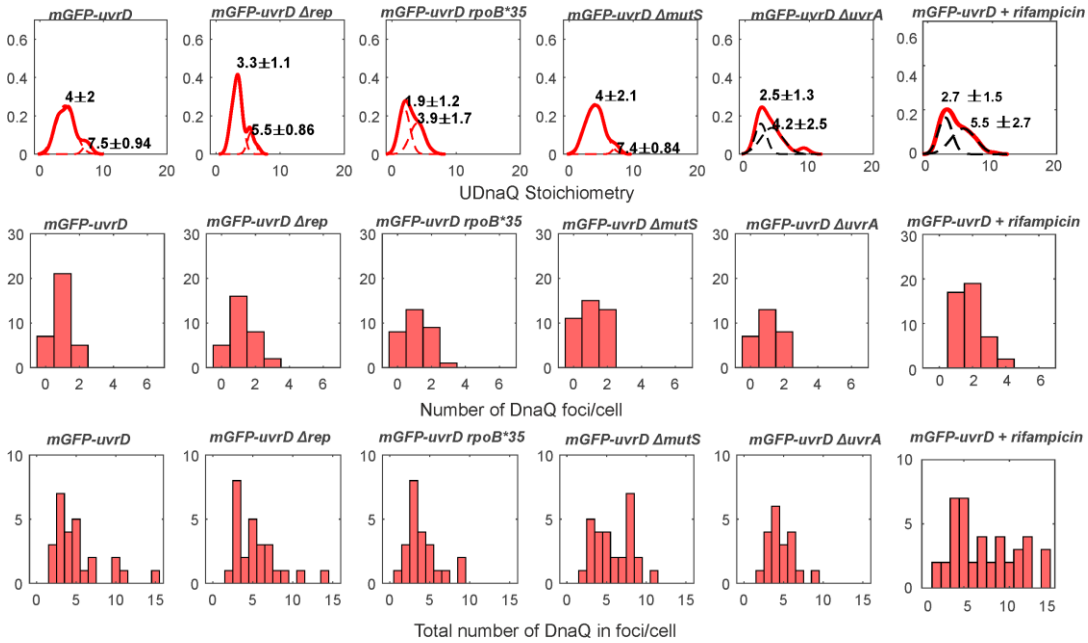

Supplementary Figure S8: DnaQ tracking characterization. Top row: Distribution of DnaQ foci stoichiometry as a kernel density estimate for all strains and conditions (red) with two Gaussian fit overlaid as black dotted lines. Peak ± half width at half maximum shown above. Middle row: Corresponding histogram of number of foci detected per cell. Bottom row: histogram of the total amount of DnaQ in foci per cell. N=30-50 cells per strain or condition.

1116

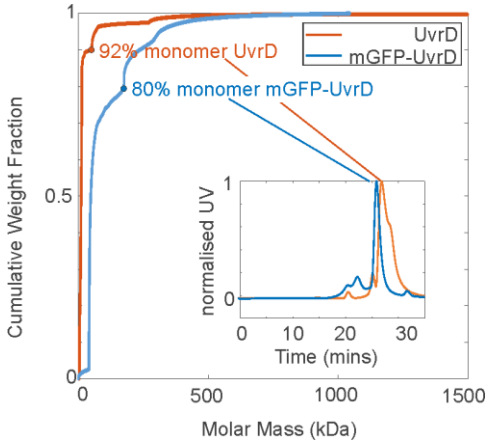

1117
1118 **Supplementary Figure S9: SEC-MALLS of UvrD/mGFP UvrD .** Size Exclusion
1119 Chromatography - Multi-Angle Laser Light Scattering (SEC-MALLS) of 4μM UvrD (red) and
1120 mGFP-UvrD (blue) cumulative weight fraction as a function of molar mass. 92% of UvrD and
1121 80% of mGFP-UvrD is consistent with a monomer. Inset shows the normalised UV
1122 abosorbance as a function of elution time through the column with the monomer peaks
1123 indicated.
1124

1125
1126

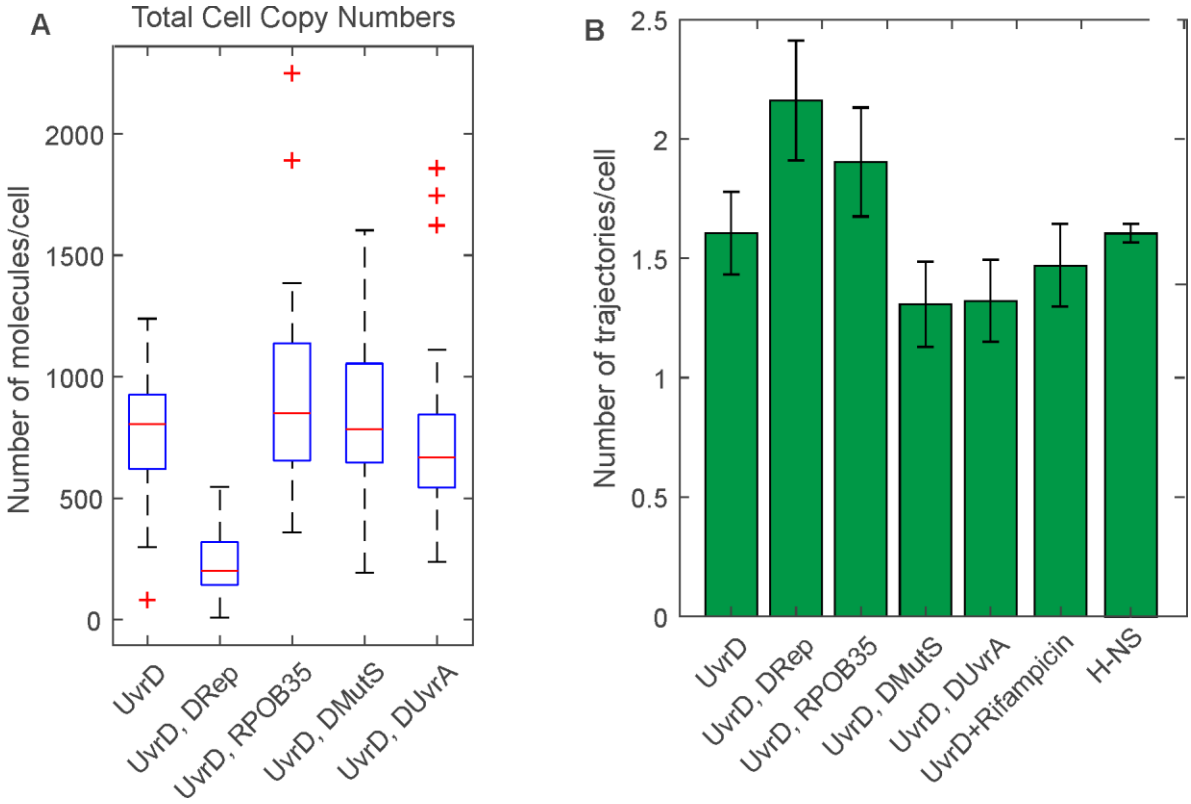

1127

1128 **Supplementary Figure S10:** A. Boxplot of the total number of mGFP-UvrD molecules per
1129 cell, estimated by numerical integration of the whole cell fluorescence. Median is shown as
1130 red line, bottom and top of the blue box mark the 25th and 75th percentiles and whiskers
1131 extend to the most extreme points not considered outliers (2.7 standard deviations covering
1132 99.3% of normally distributed data) with outliers beyond this shown as red +. N=30 cells per
1133 strain. B Number of trajectories per cell used in the stoichiometry determination
1134

1135

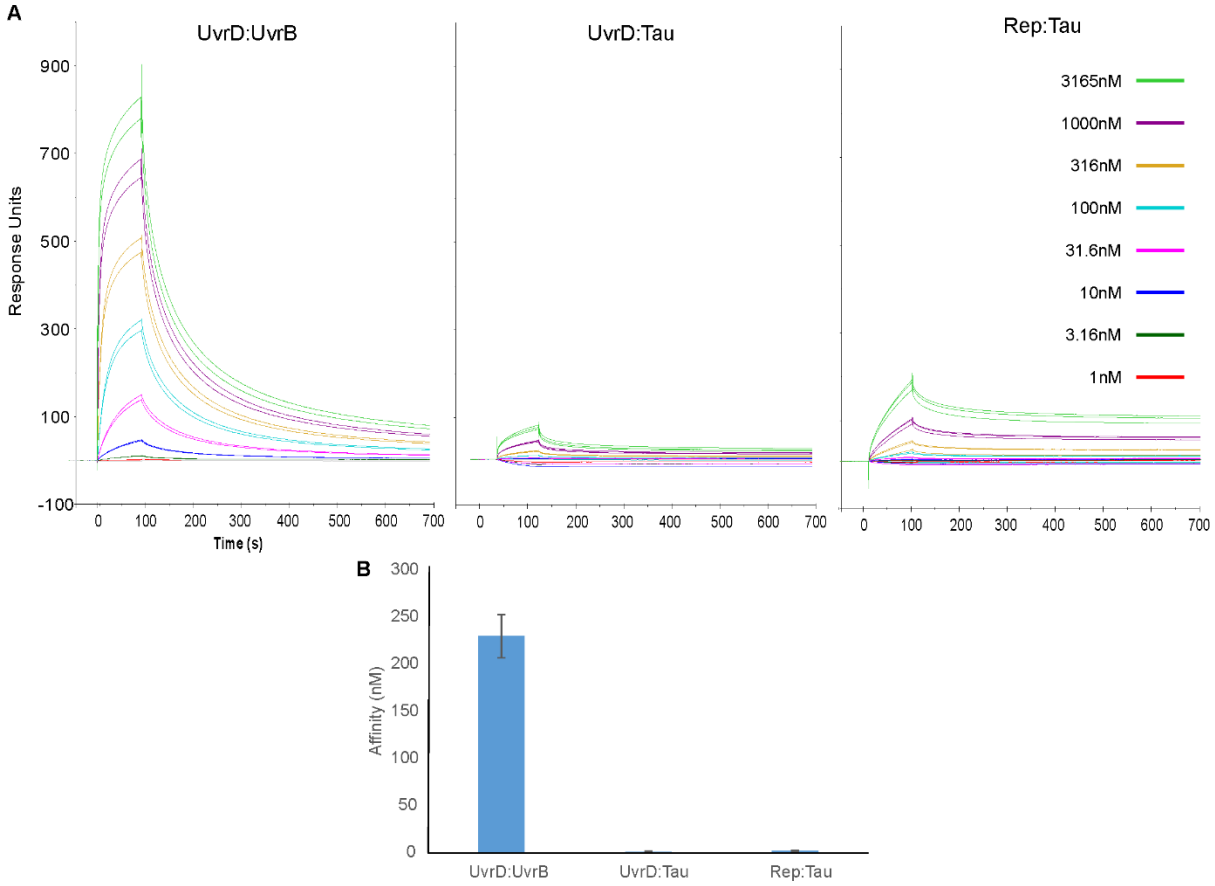

1136

1137 **Supplementary Figure S11: Surface plasmon resonance measurements of helicase**
1138 **interactions with Tau** A. Titration response curves for UvrD:UvrB, UvrD:Tau and Rep:Tau
1139 with their affinities shown in B.

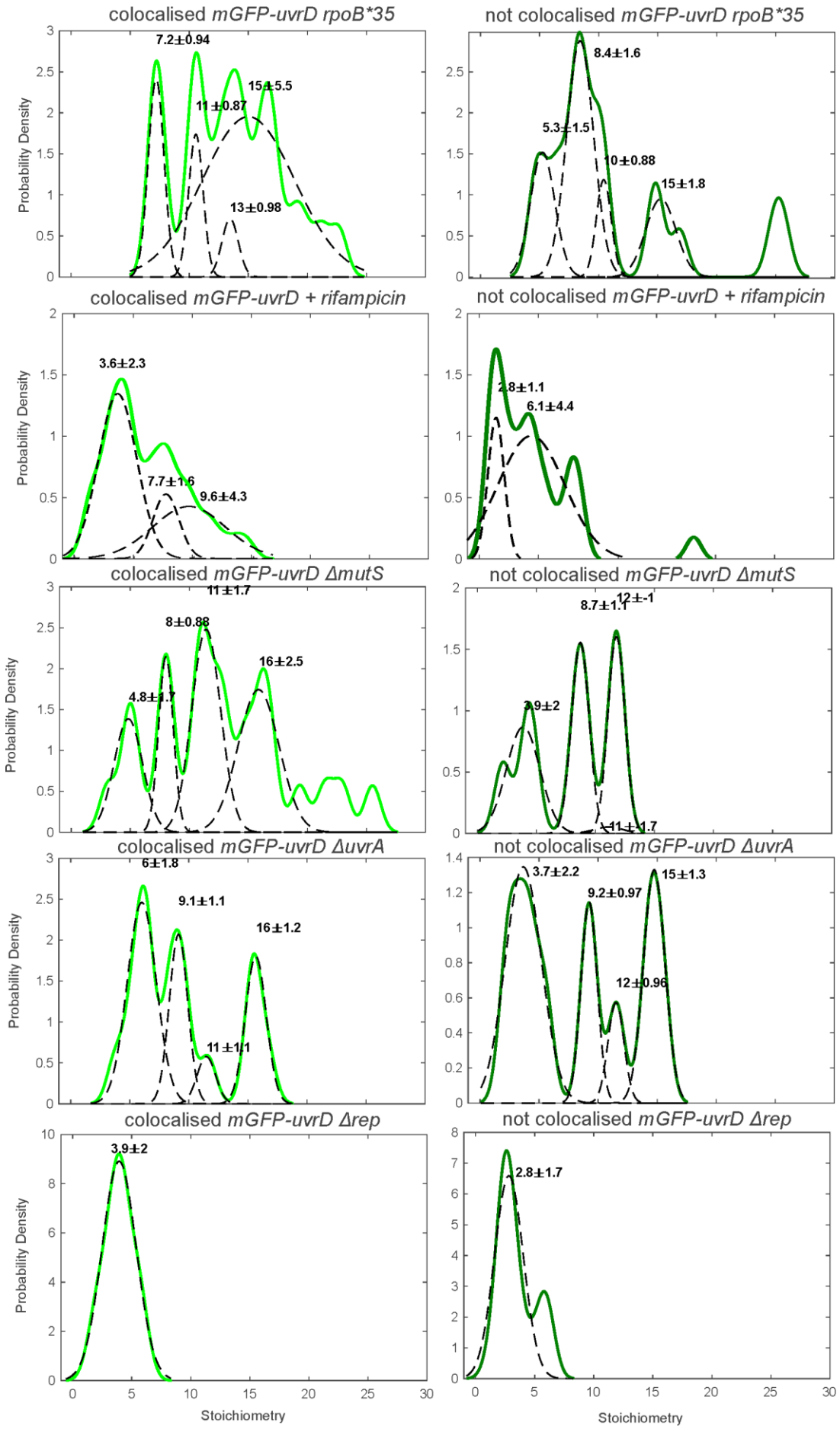
colocalised mGFP-uvrD rpoB*35
7.2±0.94
11±0.87
15±5.5
13±0.98
not colocalised mGFP-uvrD rpoB*35
8.4±1.6
5.3±1.5
10±0.88
15±1.8
colocalised mGFP-uvrD + rifampicin
3.6±2.3
7.7±1.6
9.6±4.3
not colocalised mGFP-uvrD + rifampicin
2.8±1.1
6.1±4.4
colocalised mGFP-uvrD ΔmutS
11±1.7
8±0.88
16±2.5
4.8±1.7
not colocalised mGFP-uvrD ΔmutS
8.7±1.1
12±-1
3.9±2
11±1.7
colocalised mGFP-uvrD ΔuvrA
6±1.8
9.1±1.1
16±1.2
11±1.1
not colocalised mGFP-uvrD ΔuvrA
3.7±2.2
9.2±0.97
15±1.3
12±0.96
colocalised mGFP-uvrD Δrep
3.9±2
not colocalised mGFP-uvrD Δrep
2.8±1.7
Probability Density
Stoichiometry

1140

1141 **Supplementary Figure S12:** Perturbed UvrD stoichiometry. The distribution of UvrD foci
1142 stoichiometry rendered as a kernel density estimate for foci colocalised (Left) and non-
1143 colocalised (Right) with DnaQ foci. Distributions were fitted with multiple Gaussian fits (black
1144 dotted lines) with the peak value ± half width at half maximum indicated above each peak.
1145

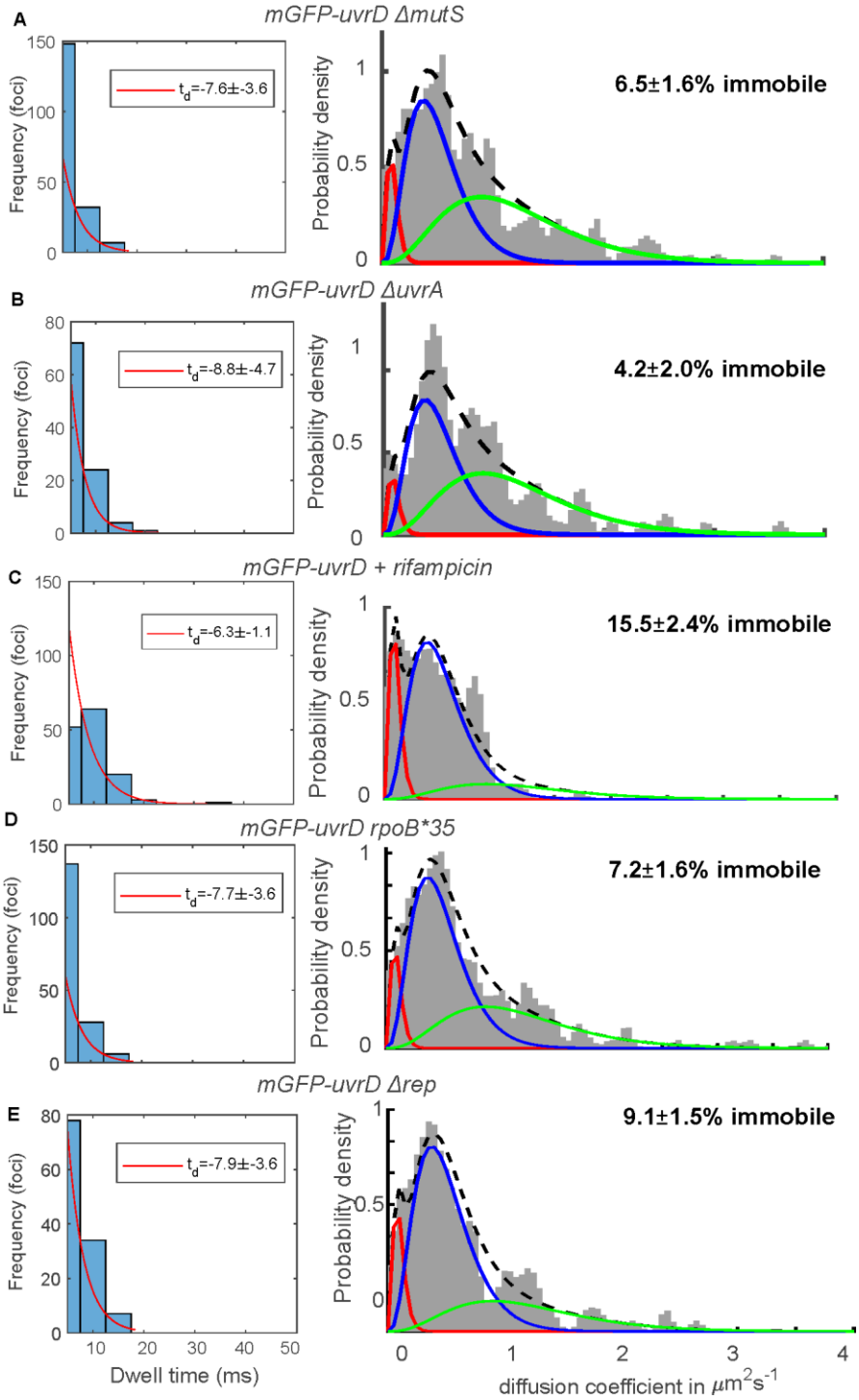

Supplementary Figure S13: UvrD perturbed dynamics. A-E Left, distribution of time UvrD and DnaQ foci were colocalised (blue) fit with an exponential (red) to yield a characteristic dwell time. Right, distribution of microscopic diffusion coefficients of UvrD foci (grey) fitted with a three state gamma distribution model containing a relatively immobile population with D = 0.1 μm^2/s (red), a transiently immobile population, D = 0.5 μm^2/s (blue) and a mobile population, D=1.2 μm^2/s (green). Errors represent 95% confidence intervals. N~300 foci/condition.

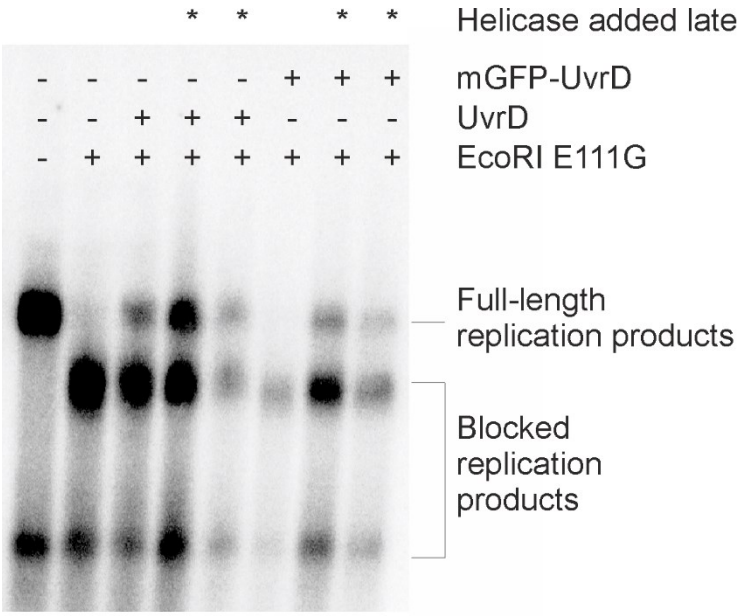

Supplementary Figure S14: In vitro replication assay using mGFP-UvrD. Denaturing agarose gel of replication products formed from pPM872 (1) in the absence and presence of EcoRI E111G block, mGFP-UvrD and UvrD added pre- and post-collision (*) as indicated.

1161 **Supplementary references**
1162
1163 1. Baba,T., Ara,T., Hasegawa,M., Takai,Y., Okumura,Y., Baba,M., Datsenko,K.A.,
1164 Tomita,M., Wanner,B.L. and Mori,H. (2006) Construction of Escherichia coli K-12 in-
1165 frame, single-gene knockout mutants: the Keio collection. *Mol. Syst. Biol.*, **2**,
1166 2006.0008.
1167 2. Bachmann,B.J. (1996) Derivations and genotypes of some mutant derivatives
1168 of Escherichia coli K-12. . In Neidhardt,F.C., Curtiss III,R., Ingraham,J.L., Lin,E.C.C.,
1169 Low,K.B., Magasanik,B., Reznikoff,W.S., Riley,M., Schaechter,M., Umbarger,H.E.
1170 (eds), *Escherichia coli and Salmonella cellular and molecular biology*. ASM Press,
1171 Washington, DC, pp. 2460–2488.
1172 3. Bernhardt,T.G. and de Boer,P.A.J. (2004) Screening for synthetic lethal mutants in
1173 Escherichia coli and identification of EnvC (YibP) as a periplasmic septal ring factor
1174 with murein hydrolase activity. *Mol. Microbiol.*, **52**, 1255–1269.
1175 4. Guy,C.P., Atkinson,J., Gupta,M.K., Mahdi,A.A., Gwynn,E.J., Rudolph,C.J., Moon,P.B.,
1176 van Knippenberg,I.C., Cadman,C.J., Dillingham,M.S., *et al.* (2009) Rep provides a
1177 second motor at the replisome to promote duplication of protein-bound DNA. *Mol.*
1178 *Cell*, **36**, 654–666.
1179 5. Syeda,A.H., Wollman,A.J.M., Hargreaves,A.L., Howard,J.A.L., Brüning,J.-G., McGlynn,P.
1180 and Leake,M.C. (2019) Single-molecule live cell imaging of Rep reveals the dynamic
1181 interplay between an accessory replicative helicase and the replisome. *Nucleic Acids*
1182 *Res.*, **47**, 6287–6298.
1183 6. Datsenko,K.A. and Wanner,B.L. (2000) One-step inactivation of chromosomal genes in
1184 *Escherichia coli* K-12 using PCR products. *Proc. Natl. Acad. Sci. USA*, **97**, 6640–
1185 6645.
1186 7. Boubakri,H., de Septenville,A.L., Viguera,E. and Michel,B. (2010) The helicases DinG,
1187 Rep and UvrD cooperate to promote replication across transcription units in vivo.
1188 *EMBO J.*, **29**, 145–157.
1189 8. Brüning,J.-G., Howard,J.A.L. and McGlynn,P. (2016) Use of streptavidin bound to
1190 biotinylated DNA structures as model substrates for analysis of nucleoprotein
1191 complex disruption by helicases. *Methods*, **108**, 48–55.
1192 9. Brüning,J.-G., Howard,J.A.L., Myka,K.K., Dillingham,M.S. and McGlynn,P. (2018) The 2B
1193 subdomain of Rep helicase links translocation along DNA with protein displacement.
1194 *Nucleic Acids Res.*, **46**, 8917–8925.
1195
1196